THE JOURNAL OF PHYSICAL CHEMISTRY C

pubs.acs.org/JPCC Article

Practical Aspects of Recording Ultra-Wideline NMR Patterns under Magic-Angle Spinning Conditions

Published as part of The Journal of Physical Chemistry virtual special issue "Hellmut Eckert Festschrift".

Adam R. Altenhof, Michael J. Jaroszewicz, Austin W. Lindquist, Lucas D. D. Foster, Stanislav L. Veinberg, and Robert W. Schurko*

Cite This: *J. Phys. Chem. C* 2020, 124, 14730−14744 Read Online

ACCESS | Metrics & More | Article Recommendations | Supporting Information

ABSTRACT: Many NMR-active nuclei give rise to solid-state NMR spectra that span extremely large frequency regions due to the effects of large anisotropic NMR interactions; such spectra, which can range from 250 kHz to several MHz in breadth, have been termed ultra-wideline (UW) NMR spectra. UWNMR spectra are often too broad to be uniformly excited by conventional pulse sequences that implement rectangular radiofrequency (RF) pulses. Therefore, they are typically acquired with specialized pulse sequences and frequency-swept (FS) pulses; however, such experiments are conducted predominantly upon stationary samples (i.e., static NMR with no magic-angle spinning, MAS). Herein, we demonstrate how to implement Carr−Purcell Meiboom−Gill (CPMG) type pulse sequences that utilize rectangular pulses to acquire high-quality wideline and UWNMR spectra under MAS conditions, which are useful for providing uniformly excited patterns with substantial signal enhancements in comparison to conventional MAS NMR spectra and identifying peaks and/or patterns corresponding to magnetically nonequivalent sites. We discuss the pulse timings, delays, and the duration of windowed acquisition periods that are necessary for using CPMG-type pulse sequences for T_2-dependent enhancement under MAS conditions while allowing for chemical shift resolution and maintaining a conventional spinning-sideband (SSB) manifold, as well as protocols for processing these spectra. Careful consideration is given to pulse lengths and RF amplitudes used in these pulse sequences. Using several spin-$^1/_2$ (i.e., ^{119}Sn, ^{207}Pb, ^{195}Pt) nuclei and one integer-spin quadrupolar nucleus (i.e., ^{2}H), we show how sensitivity-enhancing protocols, including CPMG and cross-polarization (CP), can be used to deliver high-quality MAS NMR spectra, which feature high signal-to-noise (S/N) ratios and uniformly excited SSB manifolds. The methods outlined herein are facile to implement and offer the potential to open up MAS NMR experiments to a wide variety of elements from across the periodic table.

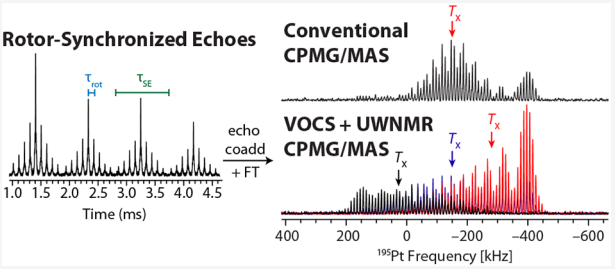

1. INTRODUCTION

There has been much recent interest in the efficient acquisition of solid-state NMR (SSNMR) spectra of unreceptive nuclei, which comprise a majority of the NMR-active nuclei in the periodic table.[1,2] Unreceptive nuclei are classified as such, due to (i) low gyromagnetic ratios (γ), (ii) low natural abundances (n.a.), (iii) dilution of the nuclide of interest, (iv) inconvenient relaxation characteristics (i.e., long longitudinal (T_1) or short transverse (T_2) relaxation time constants), and/or (v) severe inhomogeneous broadening due to large anisotropic NMR interactions (including chemical shift anisotropy (CSA), the quadrupolar interaction (QI), and/or paramagnetic broadening). Inhomogeneous broadening can produce powder patterns ranging from hundreds of kHz to several MHz in breadth; spectra of such patterns often have very low signal-to-noise (S/N), since the integrated spectral intensity is spread out over large frequency ranges. We have suggested the term *ultra-wideline (UW) NMR spectroscopy* to describe the techniques (*e.g.*, pulse sequences, frequency-swept pulses, and hardware) that are used to acquire these broad NMR powder patterns, which range in breadth from *ca.* 250 kHz to upward of 10 MHz.[2] The lower end of this range was chosen because it is generally not possible to utilize high-power rectangular pulses to provide RF amplitudes of *ca.* 250 kHz or greater with standard coil sizes (e.g., 4 mm and 5 mm) in SSNMR probes.

Aside from a strong interest in acquiring SSNMR spectra of nuclei of many elements from across the periodic table, numerous factors have contributed to the continued development and application of UWNMR methods, including the

Received: May 19, 2020
Revised: June 2, 2020
Published: June 8, 2020

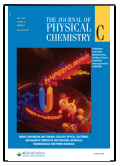

https://dx.doi.org/10.1021/acs.jpcc.0c04510
J. Phys. Chem. C 2020, 124, 14730−14744

increasing availability of high magnetic fields, new probe and accessory designs for accessing low-γ nuclei, and an array of pulse sequences designed for broadband excitation and S/N enhancement.[1−3] Our research group has focused on the latter category, working on development and application of WURST (wideband uniform-rate smooth-truncation) pulses[4] for the purposes of broadband excitation and refocusing in spin echo and Carr−Purcell/Meiboom−Gill (CPMG)-type sequences.[1,5−7] The WURST-CPMG sequence has found use for the acquisition of NMR spectra having anisotropically broadened powder patterns for a number of spin-$^1/_2$ and quadrupolar nuclei.[5,8−12] We have also explored the use of WURST pulses for broadband cross-polarization (BCP), in the form of the BRAIN-CP (broadband adiabatic inversion−cross-polarization) pulse sequence.[13]

To date, UWNMR experiments using WURST pulses and/or CPMG-type sequences have only focused upon static (i.e., stationary, nonspinning) samples; these generally yield broad static patterns of high quality, from which information on anisotropic NMR interaction tensor parameters can be extracted.[1,14,15] Powder patterns that exceed the excitation/refocusing bandwidths of any type of pulse have traditionally been acquired with a number of different field-stepped or frequency-stepped methods;[2,16−18] currently, the most commonly used method is the VOCS (variable-offset cumulative spectra) approach, in which the transmitter is stepped across the spectrum in even increments, subspectra for each step are produced by Fourier transformation, and the overall powder pattern is generated by coaddition or skyline projection.[19,20] All of the aforementioned methods work well for acquiring static UWNMR spectra of patterns representing single sites or overlapping patterns with features that make them easy to resolve. However, in situations where there are multiple magnetically nonequivalent nuclei (*i.e.*, distinct δ_{iso} values) with similar anisotropic NMR tensor parameters, it can be difficult to deconvolute the patterns underlying these spectra, and in particular, determination of δ_{iso} (and other tensor parameters, *vide infra*) can be challenging. It is possible in some cases to resolve individual patterns based on 2D relaxation-assisted separation (RAS) methods; however, these require that the nuclei have substantially different T_1 or T_2 relaxation constants.[21,22]

Magic-angle spinning (MAS) has long been used to either completely or partially average anisotropic NMR interactions in order to obtain spectra with sharp peaks, in most cases the NMR signal is consolidated under spinning-side bands (SSBs), which provides increased S/N ratios in comparison to static powder patterns.[23] This enables easy access to δ_{iso} (and in some cases the anisotropic CS parameters) as well as the quadrupolar parameters (*i.e.*, the quadrupolar coupling constant, C_Q, and the asymmetry parameter, η_Q) for certain half-integer spin and integer spin quadrupolar nuclei (N.B.: for half-integer quadrupoles, MAS is only useful for situations where the C_Q is not too large, and the combination of the MAS rate and magnetic field strength allow for clear separation of spinning sidebands from the central pattern). Importantly, in cases where experiments produce a nonuniform SSB manifold, reliable measurements of CS and quadrupolar parameters are compromised.

Unfortunately, conventional Bloch decay and spin−echo pulses sequences, and even the VOCS methodology, are often not adequate for the acquisition of high quality spectra under MAS conditions.[24,25] The CPMG sequence has been used successfully in numerous instances for the acquisition of MAS NMR spectra of both spin-$^1/_2$[26−28] and quadrupolar nuclei;[29−31] however, the majority of these studies featured the use of high-power rectangular pulses, and focused upon powder patterns with breadths smaller than 250 kHz.

There have been relatively few reports of the acquisition of directly detected UWNMR spectra under MAS conditions.[2,24,32] The primary reasons for this include: (i) difficulties in engineering probe hardware that provides extremely stable spinning speeds and magic-angle settings (see for instance, the remarkable ^{14}N (I = 1) NMR studies of Jakobsen and co-workers),[33−35] (ii) the inability to uniformly excite the entire manifold of SSBs that constitute MAS NMR spectra with high-power rectangular pulses, and (iii) challenges in achieving efficient polarization transfer (in the case of CP experiments).

Several groups of researchers have addressed the problem of acquiring wideline and UWNMR spectra under MAS conditions through the use of 2D magic-angle turning (MAT) experiments, DANTE (delays alternating with nutations for tailored excitation) pulse sequences, indirect detection schemes, and/or BCP methods. Pell et al. introduced a theoretical framework for describing the use of low-power adiabatic pulses in order to invert entire sets of SSBs arising from broad powder patterns, and experimented with these pulses for acquiring ^{77}Se MAS NMR spectra of inorganic solids.[36,37] Ideas from this work were used to design the aMAT (adiabatic magic-angle turning) experiment, which makes use of short, high-powered adiabatic pulses (SHAPs) for the acquisition of paramagnetically broadened ^{31}P MAS NMR spectra.[38] Following this, a number of MAS NMR experiments on paramagnetic solids involving variations on these experiments have been reported, for both spin-$^1/_2$ and quadrupolar nuclei.[39] For example, Hung and Gan utilized the MAT and phase-adjusted spinning sideband (MATPASS) NMR experiments for the acquisition of ^{7}Li and ^{31}P paramagnetically broadened NMR spectra.[40] MATPASS was also used for the acquisition of very broad ^{17}O NMR spectra of solid oxide fuel cell cathode materials by Grey and co-workers.[41] Bodenhausen, Amoureux, and co-workers reported a theoretical treatment describing the use of the DANTE pulse sequence for the acquisition of UWNMR spectra (examples for ^{19}F and ^{14}N were provided).[42] The use of the dipolar-HMQC (D-HMQC) pulse sequence (and several variants) for the acquisition of indirectly detected UWNMR spectra of both spin-$^1/_2$ and quadrupolar nuclei have been explored by Amoureux et al.[43,44] and Rossini et al.[45−49] Finally, Wi et al. have been carrying out studies featuring the use of BRAIN pulses for BCP to both spin-$^1/_2$ and quadrupolar nuclei (applications for UWNMR have not yet been reported).[50−53] To date, there have been no reports of a reliable method for obtaining directly detected 1D UWNMR spectra of spin-$^1/_2$ or quadrupolar nuclei using direct excitation (DE) or CP methods under MAS conditions, nor have there been any reports of implementations of CPMG-style sequences or frequency-swept pulses like WURST pulses for these purposes.

Herein, we present a preliminary study of the application of conventional and modified CPMG pulse sequences utilizing rectangular pulses for the acquisition of SSNMR spectra of spin-$^1/_2$ and integer spin nuclei with broad anisotropic patterns under MAS conditions. First, a protocol for acquiring CPMG spectra is described, which gives careful consideration to the timing of the acquisition windows and relative positions of the spin−echoes and rotational echoes−most importantly, this

https://dx.doi.org/10.1021/acs.jpcc.0c04510
J. Phys. Chem. C 2020, 124, 14730−14744

Scheme 1. Schematic Representations of the (a-i) CPMG-π, (b-i) CPMG-$\pi/2$, (c-i) CPMG-$\pi/4$, (a-ii) CPMG-πA, (b-ii) CPMG-$\pi/2$A, and (c-ii) CPMG-$\pi/4$A Pulse Sequences[a]

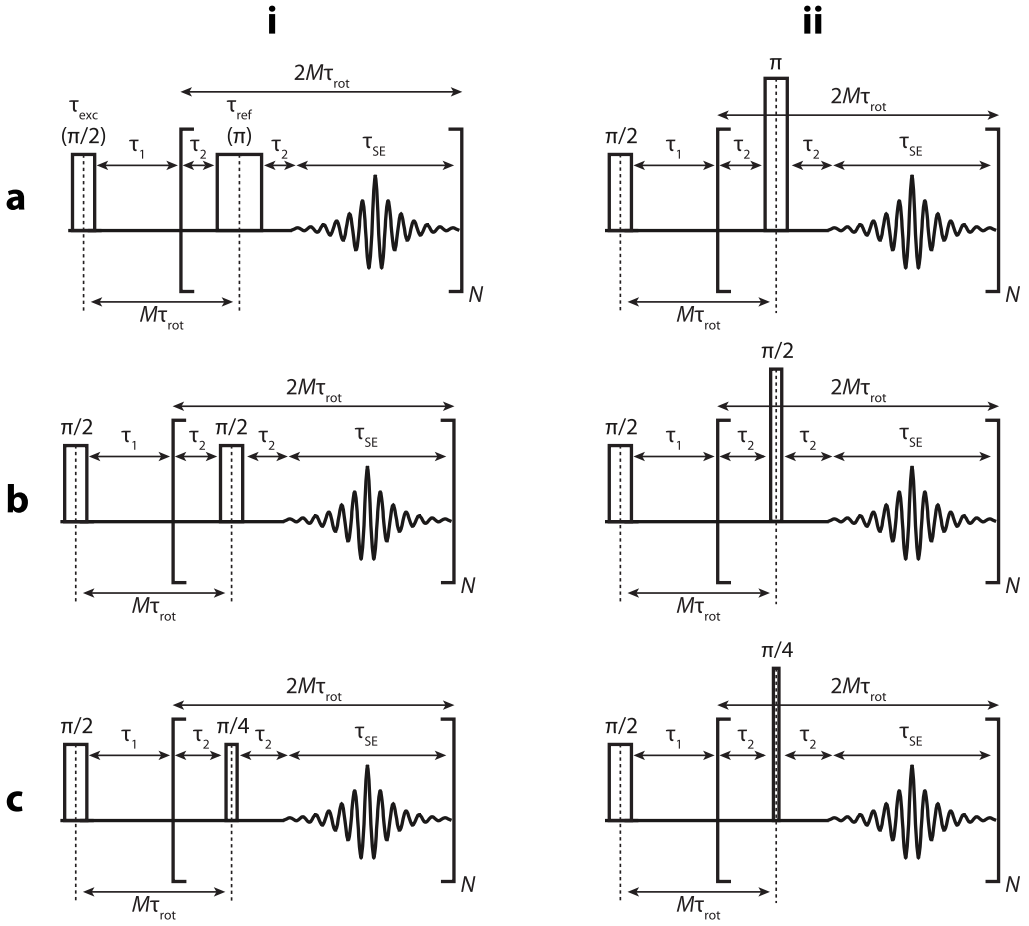

[a]In each sequence name, the refocusing pulse angle is denoted after CPMG, and the letter "A" indicates that the amplitude of the refocusing pulse is two times that of the excitation pulse. The excitation and refocusing pulse lengths are denoted by τ_{exc} and τ_{ref}, respectively. The echo delay and ring-down delays are denoted by τ_1 and τ_2, respectively. The acquisition time of a single spin echo and the rotor period are denoted by τ_{SE} and τ_{rot}, respectively. Under MAS, rotor synchronization is achieved when the duration of a single CPMG cycle, which is defined as the total time of a single refocusing pulse along with the two associated ring-down delays and the subsequent windowed spin-echo acquisition period, is an integer multiple of the rotor period (*i.e.*, when $2M\tau_{rot} = 2\tau_2 + \tau_{ref} + \tau_{SE}$ is satisfied).

protocol allows for the accurate measurement of isotropic shifts in the same manner as standard MAS and CP/MAS experiments, while affording the S/N gains associated with CPMG pulse sequences. Then, modifications to and considerations of the pulse lengths and RF amplitudes used in CPMG pulse sequences for the purpose of acquiring UWNMR spectra under MAS conditions are discussed. Experimental ^{119}Sn, ^{207}Pb, ^{195}Pt, and ^{2}H MAS NMR spectra acquired with modified CPMG pulse sequences are shown and contrasted against conventional CPMG NMR spectra acquired under MAS conditions. A brief discussion of CP methods for the acquisition of ^{1}H−^{195}Pt and ^{1}H−^{2}H CP-CPMG/MAS NMR spectra is presented. Finally, a general strategy for implementing these easy-to-use pulse sequences is outlined; this may permit broad applications of these techniques to a variety of elements across the periodic table. We note that herein, WURST pulses are not explored for these purposes, as their typical direct excitation and refocusing lengths are on the order of the rotor periods, making challenging the precise synchronization of the effective transmitter sweep with the unique frequency dependencies of individual isochromats over the course of a rotor cycle.

2. EXPERIMENTAL METHODS

2.1. Samples. Tin(II) oxide [SnO, Sigma-Aldrich], lead zirconate [$PbZrO_3$, Sigma-Aldrich], tetraamineplatinum(II) chloride monohydrate [$Pt(NH_3)_4Cl_2{\cdot}H_2O$, Sigma-Aldrich], and deuterated α-glycine [α-glycine-d_2, Cambridge Isotope Laboratories, Inc.] were purchased and used in all subsequent NMR experiments without further purification. All samples were ground into fine powders and packed in 4 mm zirconium NMR rotors.

2.2. Solid-State NMR Spectroscopy. NMR experiments were performed using a Bruker Avance III HD console with an Oxford 9.4 T ($\nu_0(^1H)$ = 400 MHz) wide-bore magnet operating at $\nu_0(^{119}Sn)$ = 149.04 MHz, $\nu_0(^{207}Pb)$ = 83.68 MHz, $\nu_0(^{195}Pt)$ = 86.015 MHz, and $\nu_0(^2H)$ = 61.40 MHz. A Varian/Chemagnetics 4 mm triple-resonance HXY magic-angle spinning (MAS) probe was used for ^{119}Sn and ^{207}Pb NMR experiments. A Varian/Chemagnetics 4 mm double-resonance HX magic-angle spinning (MAS) probe was used for ^{195}Pt and ^{2}H NMR experiments. MAS NMR spectra were acquired with spinning speeds, ν_{rot}, ranging between 5 and 12 kHz with a stability of ±1 Hz. The magic angle of the probe

https://dx.doi.org/10.1021/acs.jpcc.0c04510
J. Phys. Chem. C 2020, 124, 14730−14744

was calibrated to 54.74° by maximizing the number of rotational echoes observed in the ^{79}Br FID of KBr.

Pulse width calibrations for all nuclei were performed on their respective solution-state standards. ^{119}Sn (I = $^1/_2$) chemical shifts are referenced to neat $Sn(CH_3)_4$(l) with δ_{iso} = 0.0 ppm.[54] ^{207}Pb (I = $^1/_2$) chemical shifts are reported with respect to $Pb(CH_3)_4$(l) (δ_{iso} = 0.0 ppm) by using an aqueous solution of 0.5 M $Pb(NO_3)_2$ as a secondary standard with δ_{iso} = −2941 ppm.[55] ^{195}Pt (I = $^1/_2$) chemical shifts are referenced to 1.0 M Na_2PtCl_6(aq) with δ_{iso} = 0.0 ppm.[56] ^{2}H (I = 1) chemical shifts are referenced to D_2O(l) with δ_{iso} = 4.8 ppm.[57]

All direct excitation NMR experiments used radio frequency (RF) field strengths, $\nu_{exc/ref}$, between 25 and 150 kHz. Calibrated spin-locking fields of *ca.* 25 to 60 kHz were employed for all CP experiments. Spectra of compounds having protons were acquired using ^{1}H continuous-wave (CW) decoupling with RF fields ranging between 40 and 50 kHz. Rotor-synchronized refocusing pulses were used in all MAS experiments by ensuring the time of a single CPMG cycle (Scheme 1a-i) was an integer multiple of the rotor period (*i.e.*, by satisfying the following equation: $2M\tau_{rot} = 2\tau_2 + \tau_{ref} + \tau_{SE}$, with $2M$, τ_{rot}, τ_2, τ_{ref}, and τ_{SE} representing the number of rotor periods per CPMG cycle, the rotor period, the ring-down delay, the pulse width of the refocusing pulse, and the time of a single spin echo, respectively). Obtaining isotropic chemical shifts from CPMG-type MAS acquisitions was accomplished by encoding several *rotational echoes* within each *spin echo* (see the Results and Discussion for further explanation) in the CPMG echo trains. Each spin echo was then added together in the time domain to give a single spin−echo of length τ_{SE}, followed by removal of the dead time corresponding to the two τ_2 ring-down delay periods. This single spin echo was then apodized with Gaussian broadening in order to attenuate possible sinc wiggles in the resulting frequency-domain MAS NMR spectra. This was carried out by first positioning the Gaussian shape above the echo maximum (*i.e.*, at the center of the spin echo) and then multiplying the spin echo with this shape. This window processing procedure is referred to as *Gaussian multiplication* for brevity. One or two zero fills were then applied and a subsequent Fourier transform was used to produce the MAS NMR spectrum. Finally, either a magnitude calculation or a combination of zeroth- and first-order phase corrections were used to obtain absorptive NMR spectra (see Figures S1, S2, and S3, and the phase correction routine detailed in the Supporting Information). A full listing of all parameters used in these experiments is given in the Supporting Information, Tables S1−S9. All direct-excitation schemes employ the eight-step phase cycling scheme used by Bhattacharyya and Frydman to allow for high S/N acquisition (Figures S4 and S5).[58] All CP schemes use the 16-step phase cycling scheme used by Larsen and co-workers to allow for coherent CP transfer.[59] All pulse sequences described herein are available upon request by contacting the corresponding author.

2.3. Spectral Processing and Simulations. Data were processed using the Topspin 3.6.1 software with custom automated routines. Numerical simulations of NMR spectra were performed with the SIMPSON 4.1.1[60] software package. The average over the powder was calculated for 986 and 4180 (α, β) pairs according to the ZCW[61,62] scheme and for 100 γ angles. Phase cycling was achieved by coherence matrix filtration. Further experimental and processing details are provided in the Supporting Information and in the Results and Discussion.

3. RESULTS AND DISCUSSION

3.1. Overview. In the sections that follow, it is shown how standard pulse sequences (*vide infra*), which use CPMG loops for T_2-dependent signal enhancement, can be used to acquire high-quality UWNMR MAS NMR spectra (in terms of high S/N and uniform excitation), from which distinct δ_{iso} values can be easily identified. First, the acquisition and processing of FIDs acquired using the CPMG protocol under MAS conditions is explored via numerical simulations, and experimental results from corresponding MAS and CPMG/MAS experiments are compared. Careful consideration is given to the timing of both spin echoes and rotational echoes. Second, various modifications of CPMG-type sequences under MAS are examined, where the effects of different RF amplitudes and pulse lengths are considered. Comparisons are made between those and conventional CPMG/MAS data sets. CPMG/MAS direct excitation data sets for spin-$^1/_2$ (^{119}Sn, ^{207}Pb, ^{195}Pt) and spin-1 (^{2}H) nuclei are then presented, along with a preliminary exploration of the use of CP/CPMG pulse sequences for ^{1}H−^{195}Pt and ^{1}H−^{2}H CP/MAS experiments. Finally, the practical considerations for the usage of these methods are discussed, along with their limitations.

3.2. CPMG-MAS Pulse Sequences: Timings and Pulses. Scheme 1a-i shows the conventional CPMG pulse sequence which can be used to acquire high-quality wideline or UWNMR spectra under static conditions (*i.e.*, stationary samples with ν_{rot} = 0 kHz).[5,6,8,11,13,63−71] This sequence, along with the others pictured in Scheme 1, can also be used to acquire distortionless MAS NMR spectra of UWNMR patterns without any major modifications, with the exception of careful consideration of (i) *rotor synchronization* (*i.e.*, ensuring the time between subsequent refocusing pulses is an integer multiple of the rotor period, ν_{rot}),[27,69] and (ii) the *pulse lengths* and *RF amplitudes*. These two aspects are discussed below.

3.2.1. Timing and Rotor Synchronization. There are three timing elements that collectively form a *CPMG cycle* (Scheme 1a-i): (i) the total duration of a single *refocusing pulse* (*i.e.*, τ_{ref}), (ii) the two *ring-down delays* (*i.e.*, the τ_2 delays that flank each refocusing pulse), and (iii) the *windowed acquisition period* (*i.e.*, the time interval, τ_{SE}, in which the receiver is turned on and a spin echo is collected). The length of the CPMG cycle must be an integer multiple of τ_{rot} (i.e., $2M\tau_{rot}$), where $2M$ is an integer value representing the number of rotor periods within the CPMG cycle. Hence, the following equation must be satisfied in order to achieve rotor synchronization: $2M\tau_{rot} = 2\tau_2 + \tau_{ref} + \tau_{SE}$. The so-called *echo delay* (*i.e.*, a carefully selected delay between the excitation pulse and the first refocusing pulse, τ_1) is calculated with $\tau_1 = (\tau_{SE} - \tau_{exc})/2$, which ensures that the formation of coherent and centered spin echoes (*i.e.*, that form precisely at $\tau_{SE}/2$) throughout the duration of the entire echo train[58,69,72] and that the time between the excitation pulse and the first refocusing pulse is rotor synchronized (this holds for all the pulse sequences shown in both Scheme 1 and Scheme 2).

For CPMG data sets acquired under MAS conditions, resolving overlapping patterns and identifying their associated δ_{iso} values can be difficult, largely due to the timings of the spin echoes and rotational echoes, and the methods used for subsequent processing of the FIDs. One possible solution for resolving isotropic shifts in CPMG/MAS NMR spectra lies in

https://dx.doi.org/10.1021/acs.jpcc.0c04510
J. Phys. Chem. C 2020, 124, 14730−14744

Scheme 2. Schematic Representation of the CP-CPMG/MAS Pulse Sequence[a]

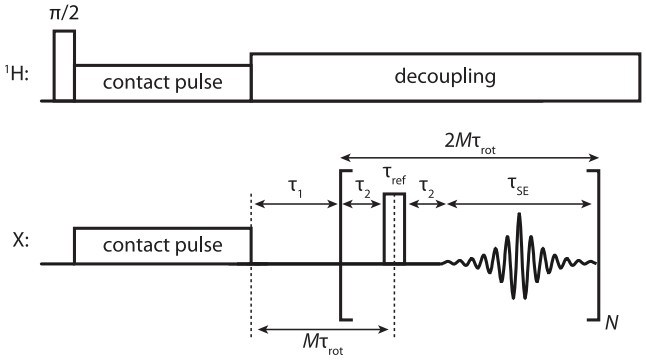

[a]The timings and parameters are consistent with the description of Scheme 1.

the consideration of the equation describing rotor synchronization (*vide supra*). Choosing a spin echo duration that is much longer than a rotor period (*i.e.*, $\tau_{SE} > \tau_{rot}$) results in the encoding of several *rotational echoes* within *each* spin echo. Then, coaddition of the spin echoes in the time domain yields a single spin echo (with duration τ_{SE}) having an increased S/N ratio from the CPMG acquisition, as well as the encoded rotational echoes that result from MAS. Removing the dead time associated with the τ_2 ring-down delays, followed by Gaussian multiplication and then Fourier transformation, results in a SSB manifold characteristic of conventional MAS NMR spectra from which the isotropic chemical shifts can be readily identified (*vide infra*).

3.2.2. Pulse Lengths and Amplitudes. When acquiring UWNMR spectra under MAS conditions using a CPMG-type sequence, careful consideration must be given to the pulse lengths and RF amplitudes, depending on the available RF power that can be applied, the pattern breadth, and the nuclear spin quantum number. There are numerous options available (see Table 1 for a summary and explanation of pulse sequence notation). The conventional CPMG pulse sequence (Scheme 1a-i), featuring a $\pi/2$-excitation pulse and a π-refocusing pulse of the same amplitude, $\nu_{exc/ref}$, but with different pulse lengths, $\tau_{ref} = 2\tau_{exc}$, is herein referred to as **CPMG-π** (the label after CPMG indicates the intended refocusing pulse tip angle). The condition $\tau_{ref} = 2\tau_{exc}$ effectively reduces the bandwidth of the refocusing pulse compared to that of the excitation pulse; the former is being executed many times over in a CPMG sequence and is therefore undesirable for the acquisition of UWNMR MAS spectra. If $\tau_{ref} = \tau_{exc}$, then there is no reduction in bandwidth during the repeated application of the refocusing pulses; however, the amplitude of the refocusing pulse must be doubled in order to maintain a π-nutation angle. Therefore, the condition $\nu_{ref} = 2\nu_{exc}$ can be used; this sequence is referred to as **CPMG-πA** (Scheme 1a-ii, the label "A" indicates that the refocusing pulse has twice the RF amplitude of the excitation pulse). For $I = 1$ nuclei, $\pi/2$-excitation and $\pi/2$-refocusing pulses are used in order to properly refocus the spin polarization under the influence of the first-order quadrupolar interaction (**CPMG-π/2**, Scheme 1b-i, N.B. this could also be relevant for acquisition of spectra of satellite transition powder patterns of half-integer quadrupolar nuclei with small C_Q values). The bandwidth of the refocusing pulse can be improved for this sequence by setting $\tau_{ref} = \tau_{exc}/2$ and $\nu_{ref} = 2\nu_{exc}$ (**CPMG-π/2A**, Scheme 1b-ii). In cases where a larger bandwidth for refocusing is desired but maximum RF amplitude is limited, a CPMG-type sequence using $\pi/2$-excitation and $\pi/4$-refocusing pulses can be executed by setting $\tau_{ref} = \tau_{exc}/2$ and $\nu_{ref} = \nu_{exc}$ (**CPMG-π/4**, Scheme 1c-i). The bandwidth of refocusing pulses for this sequence can be further improved by setting $\tau_{ref} = \tau_{exc}/4$ and $\nu_{ref} = 2\nu_{exc}$ (**CPMG-π/4A**, Scheme 1c-ii). Finally, CP-CPMG can be implemented according to Scheme 2 where the refocusing pulse after CP can be modified according to any one of the permutations described above (for example, **CP-CPMG-π/2** refers to a normal CP experiment followed by a $\pi/2$ nutation refocusing pulse).

Table 1. Definitions of the Pulse Sequences Used in This Work[a]

pulse sequence	refocusing pulse length (τ_{ref})	refocusing pulse amplitude (ν_{ref})
CPMG-π	$2\tau_{exc}$	ν_{exc}
CPMG-πA	τ_{exc}	$2\nu_{exc}$
CPMG-$\pi/2$	τ_{exc}	ν_{exc}
CPMG-$\pi/2$A	$\tau_{exc}/2$	$2\nu_{exc}$
CPMG-$\pi/4$	$\tau_{exc}/2$	ν_{exc}
CPMG-$\pi/4$A	$\tau_{exc}/4$	$2\nu_{exc}$

[a]In all cases above, the excitation pulse length and amplitude are τ_{exc} and ν_{exc}, respectively, for a tip angle of $\theta_{exc} = \pi/2$. The notation following CPMG denotes the type of refocusing pulse (π, $\pi/2$, or $\pi/4$), with the letter "A" indicating that the refocusing pulse has two times the RF amplitude of the excitation pulse.

In principle, the refocusing pulses should be as short as possible for the acquisition of UWNMR spectra with uniform patterns. If a particular refocusing tip angle is utilized to ensure a broad refocusing bandwidth and maximal signal, then the area of the rectangular pulse needs to be kept constant by increasing the RF amplitude with decreasing pulse length (*i.e.*, $\theta = 2\pi\nu_1\tau_p$). An increase in the effective bandwidth of refocusing can also be gained at the cost of signal intensity (*i.e.*, by setting as short a pulse length as possible, but without the corresponding increase in RF amplitude, resulting in a suboptimal tip angle in most cases). For example, for spin-$^1/_2$ nuclei, π-refocusing pulses are ideal, but shorter pulses with smaller tip angles could be used to increase refocusing bandwidth (*e.g.*, CPMG-$\pi/2$ or CPMG-$\pi/4$ pulse sequences); in both of these cases, there are relative losses in signal. Similarly, for spin-1 nuclei, $\pi/2$-refocusing is ideal; therefore, shorter pulses with smaller tip angles also result in increased bandwidth but relative signal losses (*e.g.*, CPMG-$\pi/4$). We note that in this work, we have chosen to initiate each sequence with a $\pi/2$ pulse, and focus on the common cases of π, $\pi/2$, and $\pi/4$ refocusing pulses; there are many other potential combinations of excitation and refocusing pulses that follow the principles outlined herein, provided that close attention is paid to pulse length and RF amplitude.

3.3. Case Studies. *3.3.1. ^{119}Sn NMR of SnO.* ^{115}Sn, ^{117}Sn, and ^{119}Sn are the three NMR-active isotopes of tin, with ^{119}Sn being the preferred isotope for NMR experimentation due to its higher natural abundance (8.58%) and larger gyromagnetic ratio ($\gamma(^{119}\text{Sn}) = -9.99760 \times 10^7$ rad T^{-1} s^{-1}, $\nu_0(^{119}\text{Sn}) =$ 149.04 MHz at 9.4 T). Despite these favorable NMR properties, acquiring high-quality ^{119}Sn NMR spectra can be challenging due to the inhomogeneous broadening that often results from large chemical shift anisotropies (CSAs). Tin(II)

https://dx.doi.org/10.1021/acs.jpcc.0c04510
J. Phys. Chem. C 2020, 124, 14730−14744

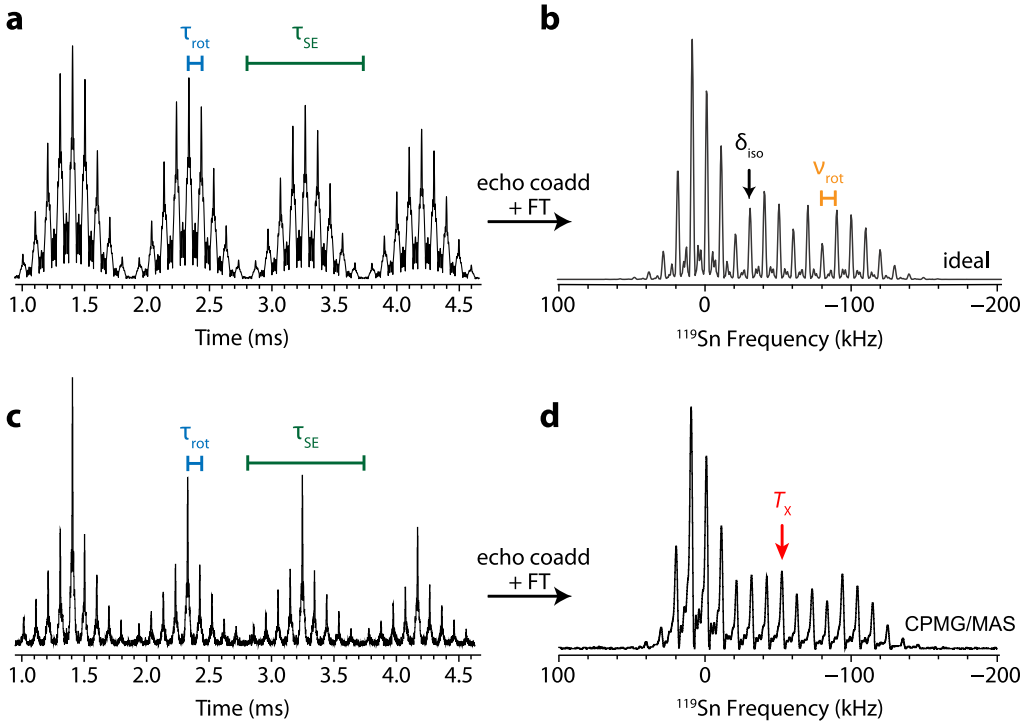

Figure 1. ^{119}Sn CPMG echo trains (left column, a and c) and the resulting MAS NMR spectra (right column, b and d) for SnO. The data sets in the top row are numerical simulations, which were simulated with the CPMG-π sequence using the NMR parameters reported in the literature (cf. main text) and the data sets in the bottom row were collected with the CPMG-π pulse sequence in 1024 scans. A spinning speed of ν_{rot} = 10 kHz (τ_{rot} = 100 μs) was used in both cases, and the transmitter offset frequency is set to *ca.* −51 kHz (*i.e.*, −51 kHz with respect to $\nu_0(^{119}Sn)$) for acquisition of all ^{119}Sn spectra (the transmitter position is indicated by T_x in the diagram). A total of 35 spin echoes (the positive magnitude of only four are shown for visual clarity) with lengths of τ_{SE} = 935 μs were collected for both echo trains (giving a *ca.* 35 ms echo train duration). An RF field strength of ν_1 = 150 kHz was used for all pulses (τ_{exc} = 1.67 μs and τ_{ref} = 3.34 μs). Rotor synchronization was achieved by setting τ_2 = 30.83 μs (ring-down delay) with M = 5. Each echo train was processed according to the procedure outlined in the Experimental Section.

oxide (abbreviated SnO) features a single magnetically distinct tin environment, which gives rise to a single CSA-dominated powder pattern (*ca.* 1000 ppm or 150 kHz at 9.4 T). This, in combination with the high tin content and relatively short longitudinal relaxation time constant, makes SnO an ideal compound for testing CPMG-type sequences under MAS conditions (though it is not truly an UWNMR spectrum). Pöppler et al. previously characterized this sample at 9.4 T under MAS (ν_{rot} = 10 kHz) using a single pulse-acquire technique, but required 9 subspectra due to limited excitation bandwidth.[73]

First, we discuss the procedure for collecting and processing CPMG/MAS NMR spectra in which the isotropic chemical shifts can be resolved. Figure 1 shows two ^{119}Sn CPMG/MAS echo trains (left column) and the resulting ^{119}Sn MAS NMR spectra (right column) for SnO. The data sets in the top row were numerically simulated using SIMPSON[74] and the data sets in the bottom row were collected with the CPMG-π pulse sequence (Scheme 1a-i). All spectra were collected at a MAS frequency of ν_{rot} = 10 kHz (corresponding to a rotor period of τ_{rot} = 100 μs). It is noted that the positive magnitude of only four spin echoes are shown for each echo train, so that the spin and rotational echoes can be visually distinguished—a total of 35 spin echoes were collected in both data sets. In addition, the points corresponding to the τ_2 ring-down delays located on both sides of each spin echo have been removed.

Figure 1a shows the times and locations of both the rotational echoes and spin echoes (indicated by the blue and green markers, respectively) in an echo train acquired with the CPMG-π sequence that was simulated with the following chemical shift tensor parameters (according to the Herzfeld Berger convention): Ω = 975 ppm, κ = 1, δ_{iso} = −208 ppm, and an indirect coupling of $^1J(^{117}Sn-^{119}Sn)$ = 8286 Hz, which accounts for some of the fine structure visible between the larger spinning sidebands.[7,75] The time between the points of maximum intensity in the adjacent spin echoes is τ_{SE} = 935 μs, about which rotational echoes form symmetrically from the periodic sample rotation occurring every 100 μs. Co-addition of each of the spin echoes in the time domain gives a single spin echo of length τ_{SE} = 935 μs, with a total of nine encoded rotational echoes. Applying Gaussian multiplication at the center of the echo followed by zero filling and Fourier transformation yields the ^{119}Sn MAS NMR spectrum (Figure 1b), in which the δ_{iso} is indicated with an arrow. Interestingly, the shape of the spinning sideband (SSB) manifold remains the same regardless of which processing method is used to obtain an absorptive NMR spectrum (*i.e.*, real phase vs magnitude processing, Figure S1). Therefore, MAS NMR spectra acquired with CPMG-type acquisitions can be processed simply and quickly with a magnitude calculation. Again, it is strongly emphasized that the spikelets comprising the pattern in the MAS NMR spectrum arise from the periodic sample rotation, as in conventional one-pulse Bloch decay MAS NMR experiments, and not from CPMG. The experimental echo train acquired with the CPMG-π sequence (Figure 1c) and the resulting ^{119}Sn MAS NMR spectrum (Figure 1d) was collected using an RF field strength of $\nu_{exc/ref}$ = 150 kHz (corresponding to excitation and refocusing pulse widths of τ_{exc} = 1.67 μs and

https://dx.doi.org/10.1021/acs.jpcc.0c04510
J. Phys. Chem. C 2020, 124, 14730−14744

τ_{ref} = 3.34 μs, respectively). These high-power pulses are required in order to uniformly excite the entire *ca.* 150 kHz SSB manifold when using the conventional CPMG-π sequence. Furthermore, the transmitter must be applied on resonance at the center of the pattern (Figure S6). Comparing this experimental spectrum with the ideal spectrum (Figure 1b) shows good agreement between the number, positions, and intensities of the SSBs.

A comparison of ^{119}Sn MAS NMR spectra collected with rotor-synchronized Hahn-echo and CPMG-π pulse sequences are shown in Figure 2. The acquisition of the ^{119}Sn MAS NMR spectrum using a conventional, rotor-synchronized, Hahn-echo pulse sequence required *ca.* 8.5 min of acquisition time (1024 scans) in order to achieve an acceptable *S*/*N* ratio and a clearly visible SSB manifold (Figure 2a). The CPMG-π experiment, conducted for the same acquisition time, gives a ^{119}Sn MAS NMR spectrum with a significantly higher *S*/*N* ratio (Figure 2b). Furthermore, the CPMG-π experiment under MAS conditions retains the information on δ_{iso}, provided that the echo train is collected and processed according to the procedure outlined above. As in the case of conventional MAS experiments with single pulses or Hahn echoes, the δ_{iso} is identified by comparison to a second ^{119}Sn CPMG-π/MAS NMR spectrum acquired at a different MAS frequency (ν_{rot} = 12 kHz, Figure 2c).

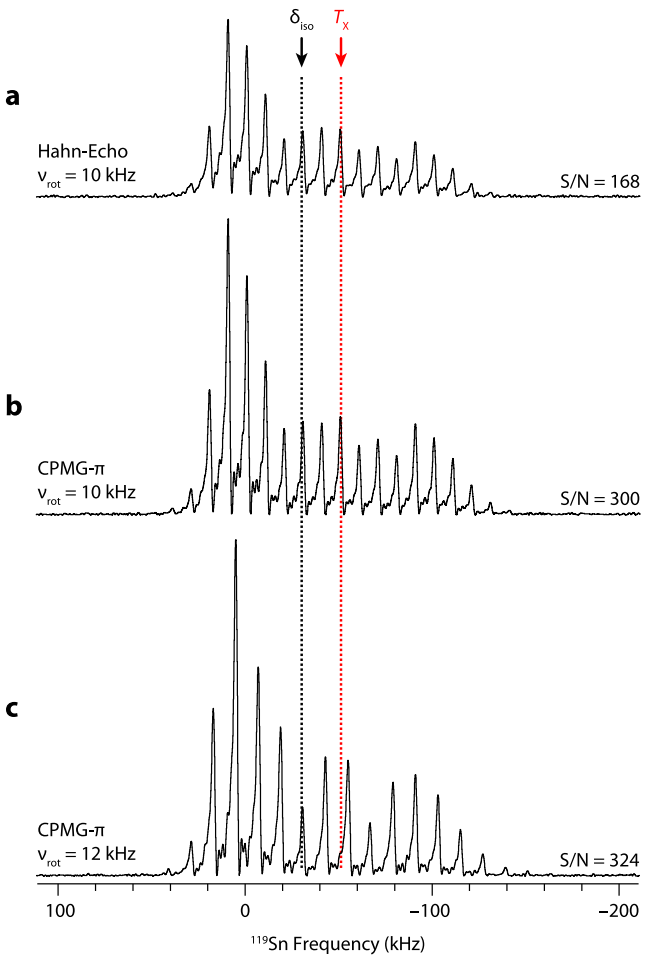

Figure 2. ^{119}Sn MAS NMR spectra of SnO acquired with the (a) Hahn echo and (b, c) CPMG-π pulse sequences (1024 scans, *ca.* 8.5 min of acquisition time). Spinning speeds of ν_{rot} = 10 kHz and 12 kHz (τ_{rot} = 100 and 83.3 μs) were used for parts a and b and for part c, respectively. The transmitter offset frequency is set to *ca.* −51 kHz (*i.e.*, −51 kHz with respect to $\nu_0(^{119}\text{Sn})$) for acquisition of all ^{119}Sn spectra (the transmitter position is indicated by T_x in the diagram). A total of 35 spin echoes were acquired with τ_{SE} = 935 μs for all experiments. For ν_{rot} = 10 kHz, *M* = 5, and τ_2 = 30.83 μs, and for ν_{rot} = 12 kHz, *M* = 6, and τ_2 = 30.63 μs. An RF field strength of ν_1 = 150 kHz was used for all pulses. Signal-to-noise (*S*/*N*) ratios are displayed on the right side of each spectrum. All spectra are represented on the same intensity scale.

It is possible to use low-power rectangular pulses to collect UWNMR spectra akin to those described above. In Figure 3, we compare NMR spectra acquired with different CPMG pulse sequences in each column, and with rectangular pulses of low, medium, and high power in each row. For low RF field strengths ($\nu_{exc/ref}$ = 25 kHz) using the conventional CPMG-π sequence (Figure 3a-i), it is clear with comparison to ideal simulations (Figure 1a), that the pattern is nonuniform, likely due to low excitation and refocusing bandwidths. This is the problem (*vide supra*) that is frequently encountered when acquiring UWNMR spectra with standard rectangular RF pulses and either Hahn-echo or CPMG pulse sequences. As the RF field strengths of the excitation and refocusing pulses increase from ν_1 = 25 to 75 kHz using the same pulse sequence (Figure 3i), the *S*/*N* ratio and the pattern bandwidth increases in the CPMG-π/MAS NMR spectra, resulting in a SSB manifold that increases in uniformity (*i.e.*, the CPMG-π sequence requires the use of high-power excitation and refocusing pulses to obtain a uniform SSB manifold). Alternatively, if the CPMG-πA sequence is used with lower-power RF pulses, then nearly the entire SSB manifold appears to be uniform (Figure 3a-ii), largely due to the shorter refocusing pulse length. As the RF field strength increases for this sequence, the SSB manifold becomes increasingly uniform and higher in *S*/*N* (Figure 3ii). A drawback to using this type of sequence is the necessity of setting $\nu_{ref} = 2\nu_{exc}$, which may not be feasible for low-γ nuclei. An alternative approach is to use the CPMG-π/4 pulse sequence. Lower-power RF fields can be used for excitation and refocusing, and by setting $\tau_{ref} = \tau_{exc}/2$ the bandwidth of refocusing is greatly improved (Figure 3a-iii). This parametrization yields a π/4 nutation angle for refocusing, which results in a loss in signal compared to π-refocusing; however, this loss is largely compensated for by using a continuous train of refocusing pulses (as in a CPMG sequence). Figure 3a-iii illustrates that with this sequence, a nearly uniform SSB manifold is produced with very short excitation and refocusing pulses of low power RF amplitudes, though with some loss in *S*/*N* compared to spectra in Figure 3a-i and Figure 3a-ii, due to the smaller nutation angle. The *S*/*N* ratio increases with higher RF fields (Figure 3iii), but again with some signal losses relative to the CPMG-π and CPMG-πA pulse sequences using similar RF field strengths due to the π/4 refocusing angle. It is important to note that these CPMG pulse sequences are superior to single-pulse excitation (*i.e.*, Bloch decay) for (i) increased *S*/*N* ratios, (ii) adequate sampling of the rotational echoes in order to fully resolve the SSB manifold (and even fine structure in the case of SnO), and (iii) the use of low power rectangular pulses (Figure S7).

3.3.2. ^{207}Pb NMR of $PbZrO_3$. ^{207}Pb is a spin-$^1/_2$ nuclide ($\gamma(^{207}\text{Pb}) = 5.58046 \times 10^7$ rad T^{-1} s^{-1}; $\nu_0(^{207}\text{Pb})$ = 83.68 MHz at 9.4 T) that often gives rise to CSA-broadened powder patterns that span hundreds of kHz in breadth.[76−78] The sample investigated in this work, $PbZrO_3$, was chosen because it has two magnetically distinct lead nuclei in the same unit cell

https://dx.doi.org/10.1021/acs.jpcc.0c04510
J. Phys. Chem. C 2020, 124, 14730−14744

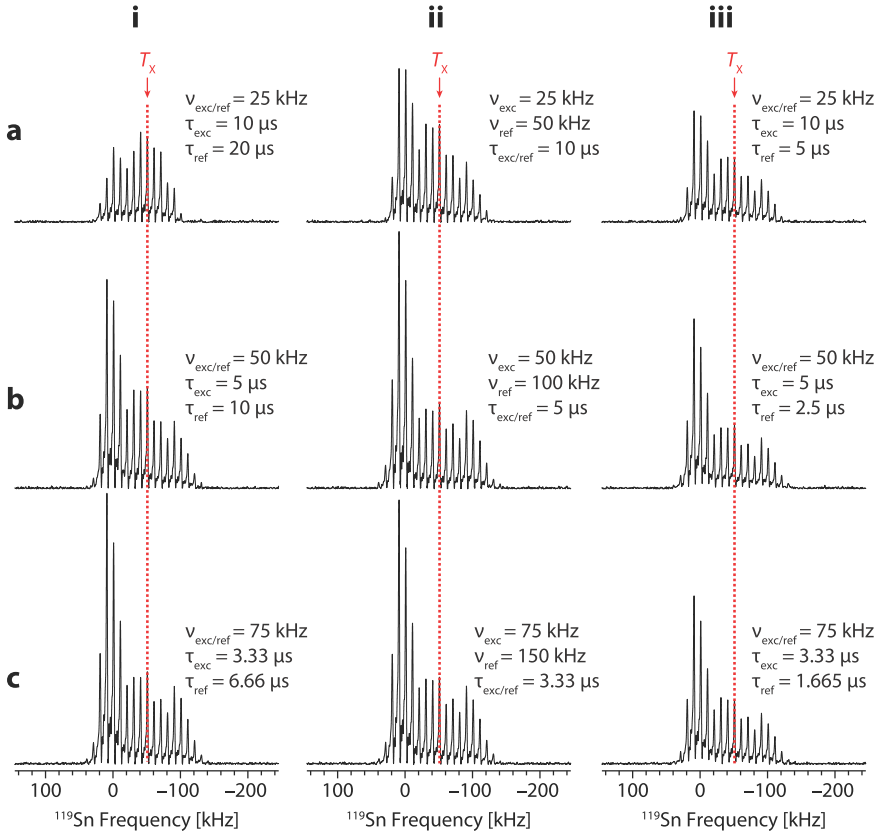

Figure 3. ^{119}Sn MAS NMR spectra of SnO acquired with the CPMG-π (column i), the CPMG-πA (column ii), and CPMG-π/4 (column iii) pulse sequences at ν_{rot} = 10 kHz in 1024 scans. Relatively low (row a), medium (row b), and high (row c) RF amplitudes are used in each case. The transmitter offset frequency is set to *ca.* −51 kHz (*i.e.*, −51 kHz with respect to $\nu_0(^{119}Sn)$) for acquisition of all ^{119}Sn spectra (the transmitter position is indicated by T_x in the diagram). A total of 35 spin echoes were acquired for all spectra with τ_{SE} = 935 μs. The RF field strengths and pulse lengths are indicated to the right of each spectrum. All spectra are represented on the same intensity scale.

that give rise to two overlapping powder patterns that are clearly distinguishable, which aids in determining if our CPMG/MAS methods can correctly determine the positions of δ_{iso} as well as the CS tensor parameters.

The ^{207}Pb NMR spectrum of $PbZrO_3$ was acquired with the WURST-CPMG pulse sequence under static conditions in *ca.* 43 min of acquisition time (Figure 4a). The numerical simulation of the ^{207}Pb MAS NMR spectrum (ν_{rot} = 11.707 kHz), which was simulated using previously reported CS tensor parameters,[79] reveals that SSB manifolds for both sites overlap, but the isotropic shifts can be clearly distinguished (Figure 4b). The experimental ^{207}Pb MAS NMR spectrum was acquired with the CPMG-π pulse sequence at an MAS frequency of ν_{rot} = 11.707 kHz and an RF field strength of ν_1 = 25 kHz (Figure 4c) in the same acquisition time as that shown in Figure 4a. Comparison of the spectra in parts b and c of Figure 4 shows that the low-power excitation and refocusing pulses, which are applied on resonance with the center of the pattern, provide inadequate excitation of the entire SSB manifold for both sites, with the intensities of the SSBs in the experimental spectrum not matching those of the ideal simulation. Interestingly, as in the case of ^{119}Sn experiments, the use of the CPMG-π/4 sequence (τ_{exc} = 10 μs; τ_{ref} = 5 μs; ν_{exc} = ν_{ref} = 25 kHz), while irradiating at the center of the pattern, results in uniform excitation of the SSB patterns for *both* sites, even when using an RF field strength as low as $\nu_{exc/ref}$ = 25 kHz (Figure 4d), thereby improving agreement with simulations. The use of low RF fields for such purposes could have great advantages in acquiring UWNMR spectra of low-γ nuclei, where high RF amplitudes are not readily available on larger 4- or 5-mm coils. Additionally, it is noted that even though the patterns are clearly distinguishable under static and MAS conditions in this particular test case, this still demonstrates that the proposed CPMG/MAS methodology can enable the identification of patterns arising from magnetically distinct sites on the basis of δ_{iso}, which can be of great value for more ambiguous situations.

3.3.3. ^{195}Pt NMR of $Pt(NH_3)_4Cl_2{\cdot}H_2O$. ^{195}Pt is a spin-$^1/_2$ nucleus that often gives rise to broad CSA-dominated powder patterns that span thousands of ppm. Ellis et al. previously reported a UWNMR MAS ^{195}Pt spectrum spanning over 1000 ppm acquired using Bloch-decay experiments, limited excitation bandwidths, and acquisition of seven subspectra at different transmitter frequencies.[24] In the current work, $Pt(NH_3)_4Cl_2{\cdot}H_2O$ is an ideal test sample for these UWNMR MAS pulse sequences because it consists of a single magnetically distinct platinum site that gives rise to a ^{195}Pt static NMR spectrum spanning *ca.* 630 kHz at 9.4 T (a true UWNMR pattern). Furthermore, this sample has protons, which enables the use of the CP pulse sequence (Scheme 2) whose experimental performance can be compared and contrasted against the direct excitation (DE) CPMG/MAS pulse sequences. Figure 5a shows the ideal ^{195}Pt NMR spectrum (ν_{rot} = 10 kHz) simulated using previously reported parameters.[13] Figure 5b shows the conventional DE CPMG-π spectrum that was acquired in 2048 scans with τ_{SE} = 935 μs,

https://dx.doi.org/10.1021/acs.jpcc.0c04510
J. Phys. Chem. C 2020, 124, 14730−14744

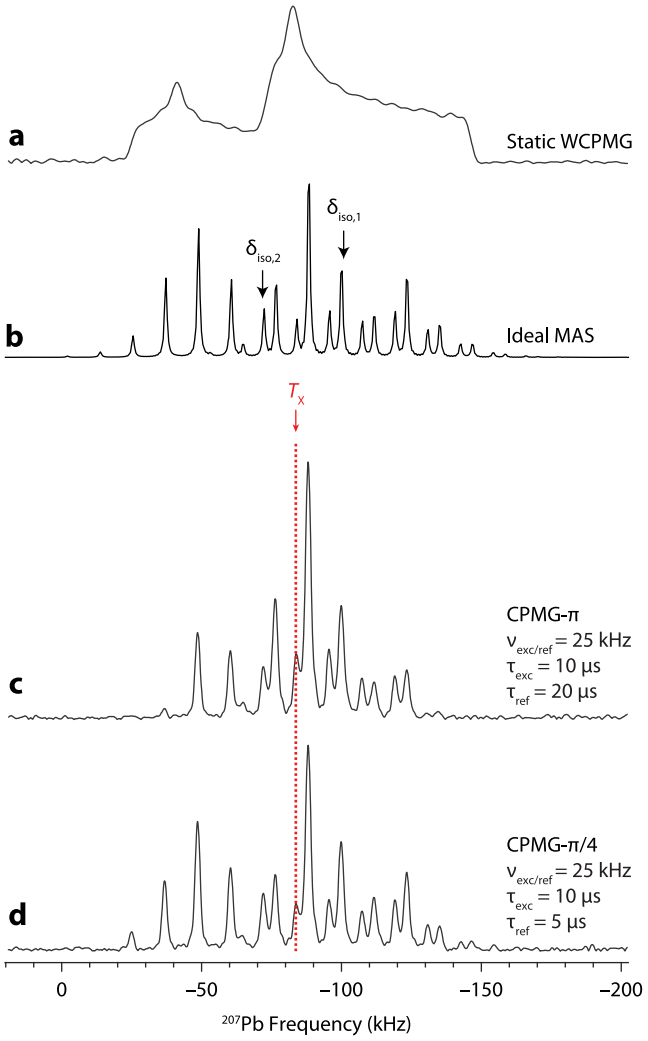

Figure 4. ^{207}Pb NMR spectrum of $PbZrO_3$ acquired under (a) static conditions with the WURST-CPMG pulse sequence (τ_p = 50 μs, $\Delta\nu$ = 1000 kHz, $\nu_{exc/ref}$ = 34 kHz). (b) Ideal ^{207}Pb MAS NMR spectrum of $PbZrO_3$ simulated at a spinning speed of ν_{rot} = 11.707 kHz using SIMPSON. Experimental ^{207}Pb MAS NMR spectra (ν_{rot} = 11.707 kHz) acquired with the (c) CPMG-π and (d) CPMG-π/4 pulse sequences. The transmitter offset frequency is set to *ca.* −83 kHz (*i.e.*, −83 kHz with respect to ν_0(^{207}Pb)) for acquisition of all ^{207}Pb spectra (the transmitter position is indicated by T_x in the diagram). All spectra were acquired using 512 scans resulting in *ca.* 42 min of acquisition time. The RF field strengths and pulse lengths are indicated to the right of each spectrum.

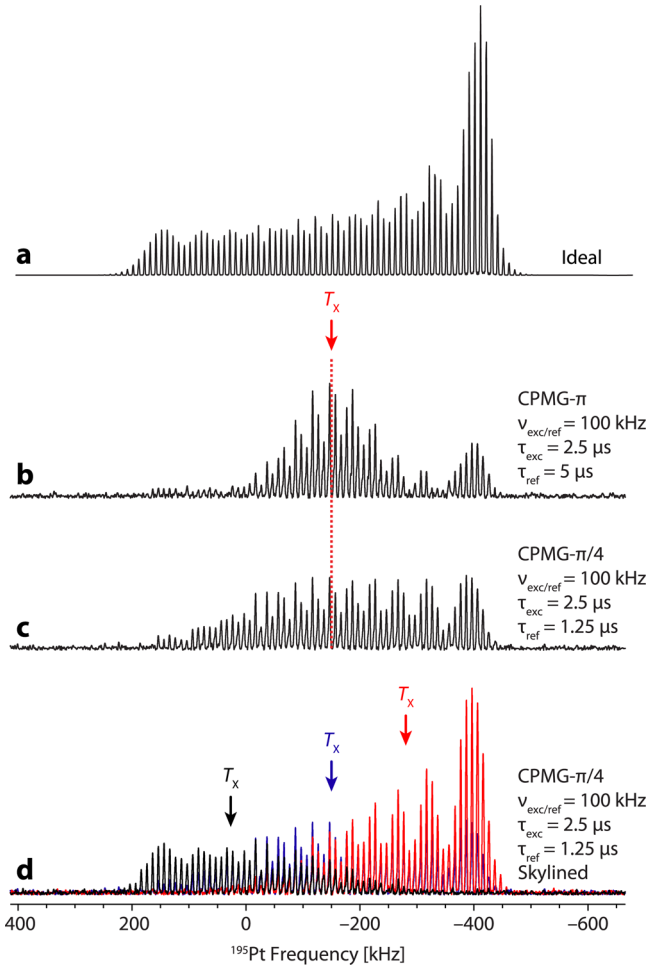

Figure 5. ^{195}Pt MAS NMR spectra of $Pt(NH_3)_4Cl_2{\cdot}H_2O$ that were (a) simulated at a spinning speed of ν_{rot} = 10 kHz using SIMPSON and experimentally acquired with the (b) CPMG-π and (c) CPMG-π/4 pulse sequences with the transmitter offset frequency set to *ca.* −150 kHz (*i.e.*, −150 kHz with respect to ν_0(^{195}Pt)) for acquisition of these ^{195}Pt spectra (the transmitter position is indicated by T_x in the diagram). (d) Experimental ^{195}Pt MAS NMR spectra (ν_{rot} = 10 kHz) acquired with the CPMG-π/4 pulse sequence at three transmitter offset frequencies (34 kHz, −150 kHz, and −286 kHz); resulting subspectra are skyline-projected on the same scale.

for which 30 spin echoes were acquired, each encoded with 9 rotational echoes. Recycle delays of 6 and 4 s were used in all ^{195}Pt DE and CP experiments, respectively, and the transmitter frequency was initially on resonance with the center of the pattern. It is clear that collecting 30 spin echoes (with τ_{SE} = 935 μs) offers acceptable sensitivity and *S*/*N*. However, even when using the highest possible RF field strengths permitted by the probe and associated electronics (ν_1 = 100 kHz), obtaining a uniform SSB manifold is not possible; a uniform manifold is only observed over the central *ca.* 100 kHz, with major distortions visible over a bandwidth of 420 kHz. Fortunately, using similar pulse sequence parameters as those used in the collection of the ^{119}Sn and ^{207}Pb CPMG/MAS NMR spectra, an increasingly uniform SSB pattern is achieved with the CPMG-π/4 pulse sequence (Figure 5c). Using the same high-power RF field strengths of ν_{exc} = ν_{ref} = 100 kHz, but with the refocusing pulse shortened to τ_{ref} = 1.25 μs, results in the uniform excitation/refocusing of isochromats associated with the central *ca.* 200 kHz of the SSB manifold, and the nonuniform excitation/refocusing of nearly the entire pattern (2048 scans). Using this new parametrization, the entire SSB manifold can be uniformly acquired using a VOCS-CPMG/MAS methodology, with only three separate transmitter locations and a skyline projection, in a total time of *ca.* 6.8 h (Figure 5d). The entire SSB manifold is uniformly excited using this three-piece acquisition strategy and matches well with the ideal simulated pattern.

Having acquired a high-quality DE ^{195}Pt CPMG/MAS NMR spectrum, optimizing the CP-CPMG/MAS pulse sequence parameters is straightforward. Figure 6b shows the ^{1}H−^{195}Pt CP-CPMG-π/2 NMR spectrum obtained with 2048 scans after optimizing the HH match and contact time with the T_x frequency at the center of the pattern. The total bandwidth corresponding to excited/refocused isochromats is only *ca.* 250

https://dx.doi.org/10.1021/acs.jpcc.0c04510
J. Phys. Chem. C 2020, 124, 14730−14744

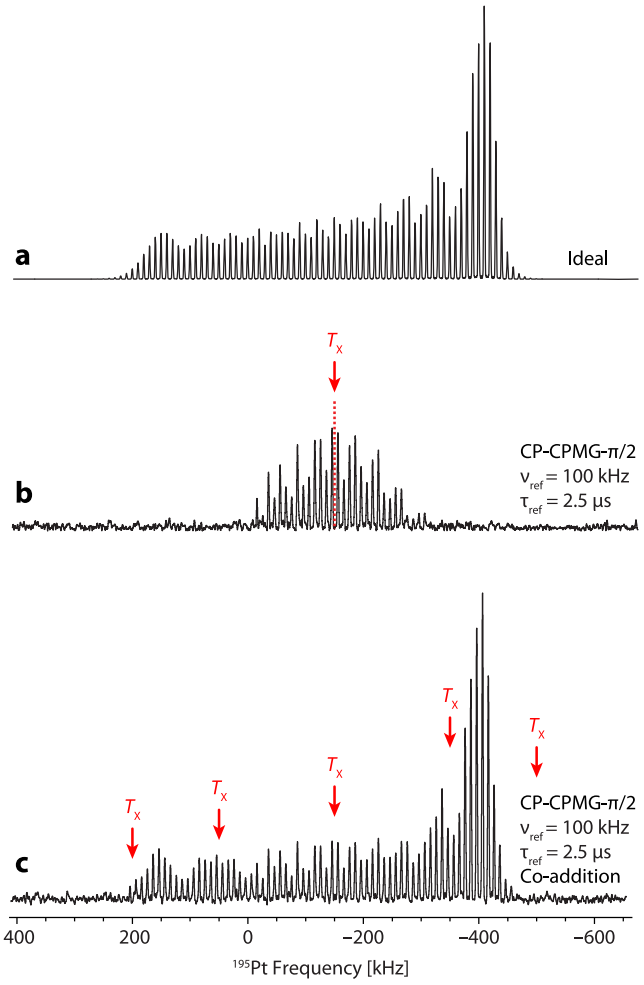

Figure 6. ^{195}Pt MAS NMR spectra of $Pt(NH_3)_4Cl_2{\cdot}H_2O$ that were (a) simulated at a spinning speed of ν_{rot} = 10 kHz using SIMPSON and experimentally acquired with the (b) CP-CPMG-π/2 pulse sequence at a single transmitter offset and (c) acquired at five transmitter offset frequencies (200, 50, −150, −350, and −500 kHz). The resulting subspectra are coadded and then plotted on the same scale.

kHz, which is substantially less than the observed minimum of *ca.* 420 kHz from the DE case. Therefore, it is likely that the bandwidth of the CP is limiting in this case rather than the pulses used for refocusing; parameters of ν_{ref} = 100 kHz and τ_{ref} = 2.5 μs are therefore sufficient. A VOCS acquisition strategy can be implemented (as for the DE case) using five evenly spaced transmitter positions. Co-adding the five subspectra (collected with 2048 scans each) yields a SSB manifold that matches well with the ideal simulated pattern (Figure 6c). In this case, efficient $T_1(^1H)$ relaxation allows for a short recycle delay, which leads to an acquisition time that is shorter than the DE case per subspectrum; however, the need for additional transmitter locations makes for a longer total acquisition time of ca. 11.4 h. Nevertheless, broad and uniform excitation of the ^{195}Pt NMR powder pattern is achieved.

These ^{195}Pt SSNMR spectra demonstrate the superior performance of the DE CPMG-π/4 pulse sequence, which delivers the highest quality data in terms of overall appearance, and excitation bandwidth. It is possible that the CP-CPMG-π/2 sequence may be superior for systems with more favorable ^{1}H relaxation parameters; investigations on other spin-$^1/_2$ nuclei with large CSAs are currently underway.

3.3.4. ^{2}H NMR of α-Glycine-d_2. ^{2}H is a spin-1 nucleus, which gives rise to SSNMR spectra that are affected by both anisotropic chemical shift and quadrupolar interactions. In particular, the spin states that give rise to the two fundamental transitions (*i.e.*, $-1 \leftrightarrow 0$ and $0 \leftrightarrow 1$) are strongly perturbed by the first-order quadrupolar interaction (FOQI), which can give rise to UWNMR spectra spanning hundreds of kHz. Analyzing the SSB manifold of ^{2}H MAS NMR spectra can provide very accurate measures of the electric field gradient (EFG) and chemical shielding (CS) tensors, which in turn provide rich chemical information. For instance, information regarding molecular-level dynamics can be obtained by acquiring and analyzing ^{2}H static and MAS NMR spectra.[80−83] Therefore, collecting ^{2}H MAS NMR spectra in which the entire SSB manifold is uniformly excited is crucial—nonuniform excitation could lead to situations in which the dynamical information contained within the ^{2}H MAS NMR spectra cannot properly be extracted.

The simulated ^{2}H MAS NMR spectrum (ν_{rot} = 10 kHz) of α-glycine-d_2 has a powder pattern that is *ca.* 250 kHz in breadth (Figure S8). Unlike ^{119}Sn, ^{207}Pb, and ^{195}Pt, the lower gyromagnetic ratio of ^{2}H (γ = 4.10663 × 10^7 rad T^{-1} s^{-1}; $\nu_0(^2H)$ = 61.402 MHz at 9.4 T) makes it challenging to obtain the necessary high-power RF field strengths required for uniform excitation of broad patterns, especially when using larger diameter coils (*e.g.*, 4 mm as in these experiments). The quadrupolar echo sequence, which features π/2 excitation and refocusing pulses, is the standard for acquiring SSNMR spectra of spin-1 nuclei like ^{2}H. This sequence and CPMG-π/2 (Scheme 1b-i), can be used to acquire both static and MAS spectra.[84] Figure 7i demonstrates that the CPMG-π/2 pulse sequence cannot uniformly excite and refocus the isochromats associated with the entire SSB manifold with RF fields $\nu_{exc/ref} \leq$ 37.5 kHz. Interestingly, the CPMG-π/2A pulse sequence provides enhanced *S*/*N* ratios and bandwidth for each RF field used compared to the standard CPMG-π/2 sequence (Figure 7ii). These enhancements owe to the shorter refocusing pulse length, τ_{ref}, as well as the higher RF field for ν_{ref} in each case (again, this might not always be feasible for low-γ nuclei and large coil diameters). The SSB manifold appears lopsided in comparison to the ideal pattern such that some of the high frequency SSBs are more intense than the lower ones; this likely results from an asymmetric response from the probe.[85] The CPMG-π/4 sequence results in a uniform SSB manifold for all RF fields (Figure 7iii). This sequence allows for low-power uniform excitation and refocusing with increased *S*/*N* ratios over conventional acquisition methods. Interestingly, no loss is observed when using the suboptimal nutation angle of π/4, as is the case for $I = {}^1/_2$ nuclei. Instead, a substantial increase is observed over π/2 refocusing in all cases. Preliminary investigations suggest this experiment closely resembles a Jeener-Broekaert type of pulse sequence, where the first π/4 pulse creates substantial dipolar order, and subsequent π/4 pulses convert the dipolar order into observable spin polarization; for the magnetically inequivalent deuterons in the $-CD_2$ group, which experience rotary resonance recoupling, this may result in enhanced Zeeman-order that is observed in each echo (N.B.: the chemical shift differences can be resolved in a sufficiently high-resolution acquisition of this pattern).[86−92] The exact mechanism of this enhancement is beyond the scope of the current work and is currently under investigation in our research group.

https://dx.doi.org/10.1021/acs.jpcc.0c04510
J. Phys. Chem. C 2020, 124, 14730−14744

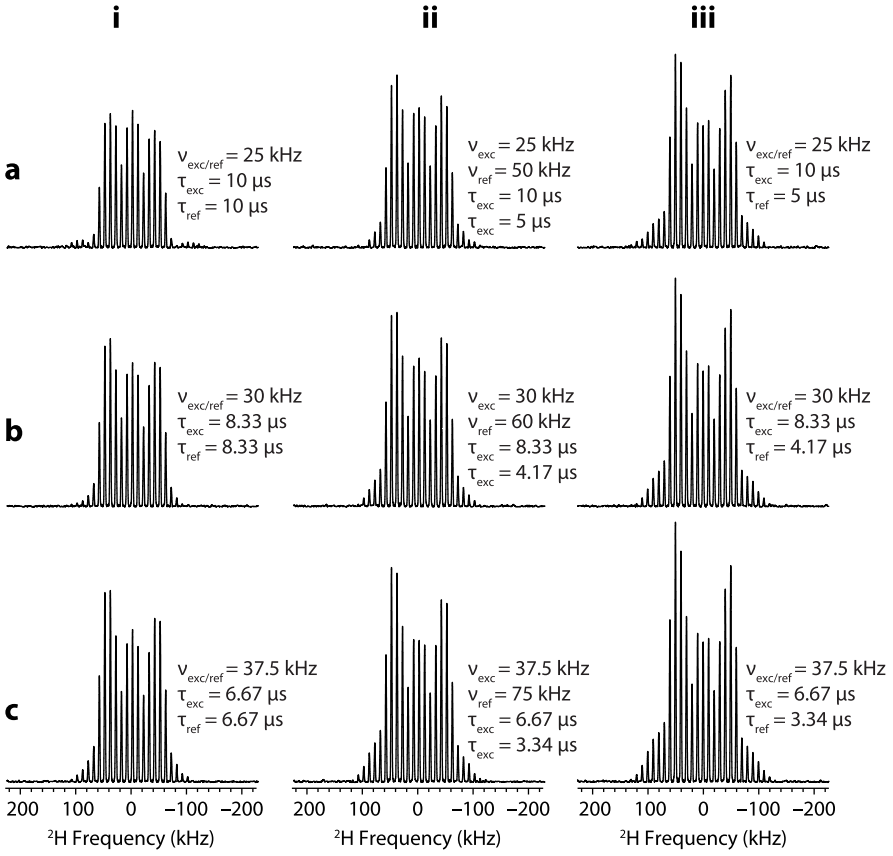

Figure 7. ^{2}H MAS NMR spectra of α-glycine-d_2 acquired with the CPMG-$\pi/2$ (column i), the CPMG-$\pi/2$A (column ii), and CPMG-$\pi/4$ (column iii) pulse sequences at ν_{rot} = 10 kHz. Relatively low (row a), medium (row b), and high (row c) RF amplitudes are used in each case. The transmitter offset frequency is set to *ca.* 0 kHz (i.e., on resonance with $\nu_0(^2H)$). 35 spin echoes were acquired for all spectra with τ_{SE} = 935 μs. The RF field strengths and pulse lengths are indicated to the right of each spectrum. All spectra are represented on the same intensity scale.

It is also possible to acquire NMR spectra of anisotropically broadened patterns with the use of CP techniques. The DE ^{2}H CPMG-$\pi/2$ NMR spectrum (ν_{rot} = 10 kHz) of α-glycine-d_2 was collected in 16 scans using an optimized recycle delay of 70 s (an acquisition time of *ca.* 18.7 min, Figure 8b), whereas the ^{1}H−^{2}H CP-CPMG-$\pi/2$ NMR spectrum was collected in 16 scans using an optimized recycle delay of 0.5 s (an acquisition time of *ca.* 8 s, Figure 8c). DE experiments revealed that the CPMG-$\pi/4$ pulse sequence is the most efficient for refocusing; therefore, CP-CPMG-$\pi/4$ was tested (Figure 8d). The resulting spectrum has higher S/N and greater uniformity than the corresponding CPMG-$\pi/2$ spectrum, and is a better match with the ideal spectrum (Figure 8a).

3.4. Experimental Guidelines, Limitations, and Practical Considerations. The results shown above demonstrate that using both CPMG and CP-CPMG pulse sequences, in conventional and modified forms, under MAS conditions is as straightforward as their use under static conditions. However, the most important factors to consider when carrying out these UWNMR MAS experiments are (i) rotor synchronization, (ii) the number of rotational echoes per spin echo, (iii) pulse lengths and amplitudes, and (iv) the subsequent processing of the echo train FIDs. Achieving rotor synchronization is possible in a number of different ways; we recommend manipulating and calculating the ring-down delays (τ_2) for given values of τ_{SE} and τ_{ref}. τ_{SE} should be chosen in such a way that the following two conditions are satisfied: (a) the resulting spin echo is composed of a whole number of points (*i.e.*, τ_{SE}/DW is an integer, where DW is the dwell time) as this is crucial for proper processing of the echo train FID, and (b) each spin echo should be sufficiently long enough to properly encode several rotational echoes (*i.e.*, $\tau_{SE} \gg \tau_{rot}$). The exact value of τ_{ref} depends on the particular pulse sequence employed. In principle, τ_{ref} should be as short as possible for any CPMG variant, but its exact value largely depends on the maximum available RF field strength (using a higher RF field strength results in overall better excitation and refocusing efficiencies), and the time resolution of the pulse programmer. After choosing suitable values for τ_{SE} and τ_{ref}, τ_2 can be calculated according to the rotor synchronization formula provided above. It is also crucial to check that $(2\tau_2 + \tau_{ref})$/DW also be a whole number, as these are the points that need to be removed between spin-echoes to allow for coaddition in data processing. Additional pulse sequence parameters, such as the transmitter frequency, RF field strengths, contact times, and spin-locking fields, should be experimentally optimized, and the values used in the collection of the MAS NMR patterns in this work serve as suitable starting conditions. Further details regarding the processing of the CPMG echo trains are provided in the Experimental Section.

There are several other important guidelines that must be considered when using the CPMG and CP-CPMG pulse sequences to acquire UWNMR spectra under MAS conditions:

(1) Given the long echo-train acquisition times required for obtaining isotropic chemical shifts from CPMG-type acquisitions, there are restrictions on the number and

https://dx.doi.org/10.1021/acs.jpcc.0c04510
J. Phys. Chem. C 2020, 124, 14730−14744

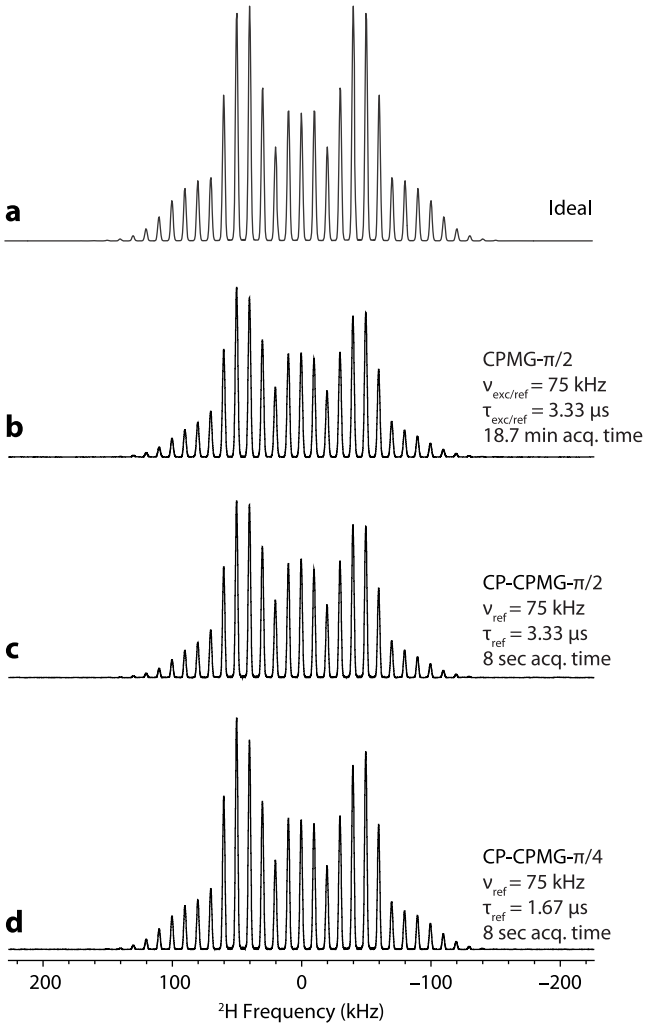

Figure 8. ^{2}H MAS NMR spectra of α-glycine-d_2 that were (a) simulated at a spinning speed of ν_{rot} = 10 kHz using SIMPSON and experimentally acquired with the (b) CPMG-π2, (c) CP-CPMG-π/2, and (d) CP-CPMG-π/4 pulse sequences. The RF field strengths, pulse lengths, and total acquisition times are indicated to the right of each spectrum. All experimental spectra are represented on the same intensity scale.

duration of the spin echoes imposed by the duty cycle that must always be considered, especially when using high-power ^{1}H decoupling. This is particularly important when spinning at moderate to slow MAS frequencies, since longer spin echoes must be acquired in order to properly encode the lengthier rotational echoes.

(2) Acquiring spin echoes that are hundreds of μs long results in correspondingly long τ_1 echo delays, which necessitates long T_2 relaxation-time constants, given the T_2 relaxation that occurs during this mandatory delay period. Fortunately, in the case of spin-$^1/_2$ nuclei affected by large CSAs, the T_2 relaxation constants are generally sufficiently long.

(3) Broader refocusing bandwidths can be achieved by using short τ_{ref} pulse lengths. In order to maintain a calibrated π-nutation angle (for spin-$^1/_2$) or π/2-nutation angle (for spin-1), shortening τ_{ref} requires the use of a higher RF field, ν_{ref}. If higher RF fields cannot be achieved, one can sacrifice signal in favor of uniform bandwidth, as demonstrated in the case of π/4-nutation for spin-$^1/_2$.

For I = 1 nuclei, π/4-refocusing should be used in the case where strong homonuclear interactions are non-negligible, as it is more efficient for obtaining high S/N and uniform pattern bandwidths (see earlier comments on Jeener-Broekaert pulse sequences). In the case where homonuclear interactions are negligible, or for I = $^1/_2$ nuclei, π/4-refocusing can still achieve more uniform pattern bandwidths, but a loss in signal should be expected.

4. CONCLUSIONS

The conventional CPMG and CP-CPMG pulse sequences, which are routinely used for collecting high-quality UWNMR patterns under static conditions, can be easily implemented and modified, to collect high-quality UWNMR patterns under MAS conditions. The major advantages of collecting CPMG NMR spectra under MAS conditions include the ability to measure isotropic chemical shifts arising from magnetically nonequivalent sites and increased S/N ratios in comparison to conventionally acquired MAS and static counterparts. Special consideration must be given to the timing of the so-called CPMG cycle, which consists of a refocusing pulse, two ring-down delays, and a windowed acquisition period, in order to ensure rotor synchronization and the subsequent coherent formation of spin echoes during the echo train ($2M\tau_{rot} = 2\tau_2 + \tau_{ref} + \tau_{SE}$). Acquisition of high-quality CPMG/MAS spectra should involve (i) collecting spin echoes that are several times longer than the rotational echoes ($\tau_{SE} \gg \tau_{rot}$), (ii) coadding all of the spin echoes into a single echo in the time domain that can be processed and Fourier transformed into a conventional MAS NMR spectrum, and (iii) ensuring the excitation and refocusing pulse bandwidths are sufficient to acquire entire SSB manifolds (this ensures that subsequent measurements of CS and quadrupolar parameter are accurate). The experimental and simulated results show that short, low-power pulses can be used to obtain uniform MAS UWNMR spectra with both direct excitation and cross-polarization methods for both spin-$^1/_2$ and integer-spin quadrupolar nuclei. These methods can be extended for the acquisition UWNMR spectra of half-integer-spin quadrupolar nuclei under MAS without any major modifications (this depends, of course, on the magnitude of the quadrupolar interaction). Increasing the power of the pulses (*i.e.*, ν_{exc} and ν_{ref}) and/or decreasing pulse widths augments the total excitation/refocusing bandwidths, and potentially lead to signal gains and/or reductions in experiment times. Clearly, these easy-to-implement pulse sequences may have a major impact in many future experiments on both spin-$^1/_2$, integer spin nuclei, and half integer spin with broad patterns arising from anisotropic chemical shift, quadrupolar, and/or paramagnetic interactions, enabling the characterization of a plethora of new materials with solid-state NMR spectroscopy.

■ ASSOCIATED CONTENT

Supporting Information

The Supporting Information is available free of charge at https://pubs.acs.org/doi/10.1021/acs.jpcc.0c04510.

Experimental parameters, additional simulations, and experiments (PDF)

https://dx.doi.org/10.1021/acs.jpcc.0c04510
J. Phys. Chem. C 2020, 124, 14730−14744

AUTHOR INFORMATION

Corresponding Author

Robert W. Schurko − *Department of Chemistry and Biochemistry, Florida State University, Tallahassee, Florida 32310, United States; National High Magnetic Field Laboratory, Tallahassee, Florida 32306, United States;* orcid.org/0000-0002-5093-400X; Phone: (850)-645-8614; Email: rschurko@fsu.edu

Authors

Adam R. Altenhof − *Department of Chemistry and Biochemistry, Florida State University, Tallahassee, Florida 32310, United States; National High Magnetic Field Laboratory, Tallahassee, Florida 32306, United States*

Michael J. Jaroszewicz − *Department of Chemistry and Biochemistry, University of Windsor, Windsor, Ontario N9B 3P4, Canada*

Austin W. Lindquist − *Department of Chemistry and Biochemistry, University of Windsor, Windsor, Ontario N9B 3P4, Canada*

Lucas D. D. Foster − *Department of Chemistry and Biochemistry, University of Windsor, Windsor, Ontario N9B 3P4, Canada*

Stanislav L. Veinberg − *Department of Chemistry and Biochemistry, University of Windsor, Windsor, Ontario N9B 3P4, Canada*

Complete contact information is available at: https://pubs.acs.org/10.1021/acs.jpcc.0c04510

Notes

The authors declare no competing financial interest.

ACKNOWLEDGMENTS

The authors thank The Florida State University and the National High Magnetic Field Laboratory for funding this research. The National High Magnetic Field Laboratory is supported by the National Science Foundation through NSF/DMR-1644779 and the State of Florida. The authors also thank the Natural Sciences and Engineering Research Council of Canada (Discovery Grant, RGPIN-2016-06642), the Canadian Foundation for Innovation, the Ontario Innovation Trust, and the University of Windsor. M.J.J. thanks the Ontario Ministry of Training, Colleges, and Universities for an Ontario Graduate Scholarship. A.W.L. thanks NSERC for an Undergraduate Student Research Assistantship and L.D.D.F. thanks the University of Windsor for support in the form of Outstanding Scholars funding.

REFERENCES

(1) Schurko, R. W. Ultra-Wideline Solid-State NMR Spectroscopy. *Acc. Chem. Res.* **2013**, *46*, 1985−1995.

(2) Schurko, R. W. Acquisition of Wideline Solid-State NMR Spectra of Quadrupolar Nuclei. *Encyclopedia of Magnetic Resonance* **2011**, 77−93.

(3) Bryce, D. L. New Frontiers for Solid-State NMR across the Periodic Table: A Snapshot of Modern Techniques and Instrumentation. *Dalt. Trans.* **2019**, *48*, 8014−8020.

(4) Kupce, E.; Freeman, R. Adiabatic Pulses for Wideband Inversion and Broadband Decoupling. *J. Magn. Reson., Ser. A* **1995**, *115*, 273−276.

(5) O'Dell, L. A.; Schurko, R. W. QCPMG Using Adiabatic Pulses for Faster Acquisition of Ultra-Wideline NMR Spectra. *Chem. Phys. Lett.* **2008**, *464*, 97−102.

(6) O'Dell, L. A.; Rossini, A. J.; Schurko, R. W. Acquisition of Ultra-Wideline NMR Spectra from Quadrupolar Nuclei by Frequency Stepped WURST-QCPMG. *Chem. Phys. Lett.* **2009**, *468*, 330−335.

(7) MacGregor, A. W.; O'Dell, L. A.; Schurko, R. W. New Methods for the Acquisition of Ultra-Wideline Solid-State NMR Spectra of Spin-1/2 Nuclides. *J. Magn. Reson.* **2011**, *208*, 103−113.

(8) Lucier, B. E. G.; Johnston, K. E.; Xu, W.; Hanson, J. C.; Senanayake, S. D.; Yao, S.; Bourassa, M. W.; Srebro, M.; Autschbach, J.; Schurko, R. W. Unravelling the Structure of Magnus' Pink Salt. *J. Am. Chem. Soc.* **2014**, *136*, 1333−1351.

(9) Tang, J. A.; O'Dell, L. A.; Aguiar, P. M.; Lucier, B. E. G.; Sakellariou, D.; Schurko, R. W. Application of Static Microcoils and WURST Pulses for Solid-State Ultra-Wideline NMR Spectroscopy of Quadrupolar Nuclei. *Chem. Phys. Lett.* **2008**, *466*, 227−234.

(10) Bonhomme, C.; Gervais, C.; Folliet, N.; Pourpoint, F.; Coelho Diogo, C.; Lao, J.; Jallot, E.; Lacroix, J.; Nedelec, J.-M.; Iuga, D.; et al. 87Sr Solid-State NMR as a Structurally Sensitive Tool for the Investigation of Materials: Antiosteoporotic Pharmaceuticals and Bioactive Glasses. *J. Am. Chem. Soc.* **2012**, *134*, 12611−12628.

(11) Perras, F. A.; Viger-Gravel, J.; Burgess, K. M. N.; Bryce, D. L. Signal Enhancement in Solid-State NMR of Quadrupolar Nuclei. *Solid State Nucl. Magn. Reson.* **2013**, *51*−*52*, 1−15.

(12) Altenhof, A. R.; Lindquist, A. W.; Foster, L. D. D.; Holmes, S. T.; Schurko, R. W. On the Use of Frequency-Swept Pulses and Pulses Designed with Optimal Control Theory for the Acquisition of Ultra-Wideline NMR Spectra. *J. Magn. Reson.* **2019**, *309*, 106612.

(13) Harris, K. J.; Lupulescu, A.; Lucier, B. E. G.; Frydman, L.; Schurko, R. W. Broadband Adiabatic Inversion Pulses for Cross Polarization in Wideline Solid-State NMR Spectroscopy. *J. Magn. Reson.* **2012**, *224*, 38−47.

(14) Siegel, R.; Nakashima, T. T.; Wasylishen, R. E. Application of Multiple-Pulse Experiments to Characterize Broad NMR Chemical-Shift Powder Patterns from Spin- 1/2 Nuclei in the Solid State. *J. Phys. Chem. B* **2004**, *108*, 2218−2226.

(15) Siegel, R.; Nakashima, T. T.; Wasylishen, R. E. Sensitivity Enhancement of NMR Spectra of Half-Integer Quadrupolar Nuclei in the Solid State via Population Transfer. *Concepts Magn. Reson., Part A* **2005**, *26A*, 47−61.

(16) Bastow, T. J.; Smith, M. E. 91Zr NMR Characterisation of Phases in Transformation Toughened Zirconia. *Solid State Nucl. Magn. Reson.* **1992**, *1*, 165−174.

(17) Kennedy, M. A.; Vold, R. L.; Vold, R. R. Stepped-Frequency NMR Spectroscopy. *J. Magn. Reson.* **1991**, *92*, 320−331.

(18) Pell, A. J.; Clément, R. J.; Grey, C. P.; Emsley, L.; Pintacuda, G. Frequency-Stepped Acquisition in Nuclear Magnetic Resonance Spectroscopy under Magic Angle Spinning. *J. Chem. Phys.* **2013**, *138*, 114201.

(19) Massiot, D.; Farnan, I.; Gautier, N.; Trumeau, D.; Trokiner, A.; Coutures, J. P. 71Ga and 69Ga Nuclear Magnetic Resonance Study of β-Ga2O3: Resolution of Four- and Six-Fold Coordinated Ga Sites in Static Conditions. *Solid State Nucl. Magn. Reson.* **1995**, *4*, 241−248.

(20) Medek, A.; Frydman, V.; Frydman, L. 59Co NMR Studies of Diamagnetic Porphyrin Complexes in the Solid Phase. *J. Phys. Chem. B* **1997**, *101*, 8959−8966.

(21) Lupulescu, A.; Kotecha, M.; Frydman, L. Relaxation-Assisted Separation of Chemical Sites in NMR Spectroscopy of Static Solids. *J. Am. Chem. Soc.* **2003**, *125*, 3376−3383.

(22) Jaroszewicz, M. J.; Frydman, L.; Schurko, R. W. Relaxation-Assisted Separation of Overlapping Patterns in Ultra-Wideline NMR Spectra. *J. Phys. Chem. A* **2017**, *121*, 51−65.

(23) Andrew, E. R.; Bradbury, A.; Eades, R. G. Nuclear Magnetic Eesonance Spectra From a Crystal Rotated at High Speed. *Nature* **1958**, *182*, 1659.

(24) Sparks, S. W.; Ellis, P. D. 195Pt Shielding Tensors in Potassium Hexachloroplatinate(IV) and Potassium Tetrachloroplatinate(II). *J. Am. Chem. Soc.* **1986**, *108*, 3215−3218.

(25) Briand, G. G.; Smith, A. D.; Schatte, G.; Rossini, A. J.; Schurko, R. W. Probing Lead(II) Bonding Environments in 4-Substituted

Pyridine Adducts of (2,6-Me2C6H3S)2Pb: An X-Ray Structural and Solid-State 207Pb NMR Study. *Inorg. Chem.* **2007**, *46*, 8625−8637.
(26) Larsen, F. H.; Farnan, I. 29Si and 17O (Q)CPMG-MAS Solid-State NMR Experiments as an Optimum Approach for Half-Integer Nuclei Having Long T1 Relaxation Times. *Chem. Phys. Lett.* **2002**, *357*, 403−408.
(27) Wiench, J. W.; Lin, V. S.-Y.; Pruski, M. 29Si NMR in Solid State With CPMG Acquisition Under MAS. *J. Magn. Reson.* **2008**, *193*, 233−242.
(28) Deschamps, M.; Roiland, C.; Bureau, B.; Yang, G.; Le Pollès, L.; Massiot, D. 77Se Solid-State NMR Investigations on AsxSe1−x Glasses Using CPMG Acquisition Under MAS. *Solid State Nucl. Magn. Reson.* **2011**, *40*, 72−77.
(29) Larsen, F. H.; Jakobsen, H. J.; Ellis, P. D.; Nielsen, N. C. QCPMG-MAS NMR of Half-Integer Quadrupolar Nuclei. *J. Magn. Reson.* **1998**, *131*, 144−147.
(30) Larsen, F. H.; Jakobsen, H. J.; Ellis, P. D.; Nielsen, N. C. High-Field QCPMG-MAS NMR of Half-Integer Quadrupolar Nuclei With Large Quadrupole Couplings. *Mol. Phys.* **1998**, *95*, 1185−1195.
(31) Larsen, F. H.; Farnan, I. Site Populations and Short Range Order in Aluminosilicates Investigated by 27Al Solid-State NMR. *J. Phys. Chem. B* **2004**, *108*, 9764−9771.
(32) Thibault, M. H.; Lucier, B. E. G.; Schurko, R. W.; Fontaine, F. G. Synthesis and Solid-State Characterization of Platinum Complexes with Hexadentate Amino- and Iminophosphine Ligands. *Dalt. Trans.* **2009**, No. No, 7701−7716.
(33) Jakobsen, H. J.; Hove, A. R.; Hazell, R. G.; Bildsøe, H.; Skibsted, J. Solid-State 14N MAS NMR of Ammonium Ions as a Spy to Structural Insights for Ammonium Salts. *Magn. Reson. Chem.* **2006**, *44*, 348−356.
(34) Giavani, T.; Bildsøe, H.; Skibsted, J.; Jakobsen, H. J. A Solid-State 14N Magic-Angle Spinning NMR Study of Some Amino Acids. *J. Magn. Reson.* **2004**, *166*, 262−272.
(35) Jakobsen, H. J.; Hove, A. R.; Bildsøe, H.; Skibsted, J.; Brorson, M. Long-Term Stability of Rotor-Controlled MAS Frequencies to 0.1 Hz Proved by 14N MAS NMR Experiments and Simulations. *J. Magn. Reson.* **2007**, *185*, 159−163.
(36) Pell, A. J.; Kervern, G.; Emsley, L.; Deschamps, M.; Massiot, D.; Grandinetti, P. J.; Pintacuda, G. Broadband Inversion for MAS NMR with Single-Sideband-Selective Adiabatic Pulses. *J. Chem. Phys.* **2011**, *134*, 024117.
(37) Sanders, K. J.; Pell, A. J.; Wegner, S.; Grey, C. P.; Pintacuda, G. Broadband MAS NMR Spectroscopy in the Low-Power Limit. *Chem. Phys. Lett.* **2018**, *697*, 29−37.
(38) Clément, R. J.; Pell, A. J.; Middlemiss, D. S.; Strobridge, F. C.; Miller, J. K.; Whittingham, M. S.; Emsley, L.; Grey, C. P.; Pintacuda, G. Spin-Transfer Pathways in Paramagnetic Lithium Transition-Metal Phosphates from Combined Broadband Isotropic Solid-State MAS NMR Spectroscopy and DFT Calculations. *J. Am. Chem. Soc.* **2012**, *134*, 17178−17185.
(39) Pell, A. J.; Pintacuda, G. Broadband Solid-State MAS NMR of Paramagnetic Systems. *Prog. Nucl. Magn. Reson. Spectrosc.* **2015**, *84*−*85*, 33−72.
(40) Hung, I.; Edwards, T.; Sen, S.; Gan, Z. MATPASS/CPMG: A Sensitivity Enhanced Magic-Angle Spinning Sideband Separation Experiment for Disordered Solids. *J. Magn. Reson.* **2012**, *221*, 103−109.
(41) Halat, D. M.; Dervişoğlu, R.; Kim, G.; Dunstan, M. T.; Blanc, F.; Middlemiss, D. S.; Grey, C. P. Probing Oxide-Ion Mobility in the Mixed Ionic−Electronic Conductor La2NiO4+δ by Solid-State 17O MAS NMR Spectroscopy. *J. Am. Chem. Soc.* **2016**, *138*, 11958−11969.
(42) Lu, X.; Trébosc, J.; Lafon, O.; Carnevale, D.; Ulzega, S.; Bodenhausen, G.; Amoureux, J.-P. Broadband Excitation in Solid-State NMR Using Interleaved DANTE Pulse Trains With N Pulses per Rotor Period. *J. Magn. Reson.* **2013**, *236*, 105−116.
(43) Shen, M.; Trébosc, J.; O'Dell, L. A.; Lafon, O.; Pourpoint, F.; Hu, B.; Chen, Q.; Amoureux, J.-P. Comparison of Various NMR Methods for the Indirect Detection of Nitrogen-14 Nuclei via Protons in Solids. *J. Magn. Reson.* **2015**, *258*, 86−95.
(44) Shen, M.; Trébosc, J.; Lafon, O.; Gan, Z.; Pourpoint, F.; Hu, B.; Chen, Q.; Amoureux, J.-P. Solid-State NMR Indirect Detection of Nuclei Experiencing Large Anisotropic Interactions Using Spinning Sideband-Selective Pulses. *Solid State Nucl. Magn. Reson.* **2015**, *72*, 104−117.
(45) Rossini, A. J.; Hanrahan, M. P.; Thuo, M. Rapid Acquisition of Wideline MAS Solid-State NMR Spectra with Fast MAS, Proton Detection, and Dipolar HMQC Pulse Sequences. *Phys. Chem. Chem. Phys.* **2016**, *18*, 25284−25295.
(46) Perras, F. A.; Venkatesh, A.; Hanrahan, M. P.; Goh, T. W.; Huang, W.; Rossini, A. J.; Pruski, M. Indirect Detection of Infinite-Speed MAS Solid-State NMR Spectra. *J. Magn. Reson.* **2017**, *276*, 95−102.
(47) Venkatesh, A.; Ryan, M. J.; Biswas, A.; Boteju, K. C.; Sadow, A. D.; Rossini, A. J. Enhancing the Sensitivity of Solid-State NMR Experiments with Very Low Gyromagnetic Ratio Nuclei with Fast Magic Angle Spinning and Proton Detection. *J. Phys. Chem. A* **2018**, *122*, 5635−5643.
(48) Venkatesh, A.; Hanrahan, M. P.; Rossini, A. J. Proton Detection of MAS Solid-State NMR Spectra of Half-Integer Quadrupolar Nuclei. *Solid State Nucl. Magn. Reson.* **2017**, *84*, 171−181.
(49) Venkatesh, A.; Hung, I.; Boteju, K. C.; Sadow, A. D.; Gor'kov, P. L.; Gan, Z.; Rossini, A. J. Suppressing 1H Spin Diffusion in Fast MAS Proton Detected Heteronuclear Correlation Solid-State NMR Experiments. *Solid State Nucl. Magn. Reson.* **2020**, *105*, 101636.
(50) Wi, S.; Gan, Z.; Schurko, R.; Frydman, L. Cross-Polarization Phenomena in the NMR of Fast Spinning Solids Subject to Adiabatic Sweeps. *J. Chem. Phys.* **2015**, *142*, 064201.
(51) Wi, S.; Schurko, R.; Frydman, L. 1H-2H Cross-Polarization NMR in Fast Spinning Solids by Adiabatic Sweeps. *J. Chem. Phys.* **2017**, *146*, 104201.
(52) Wi, S.; Kim, C.; Schurko, R.; Frydman, L. Adiabatic Sweep Cross-Polarization Magic-Angle-Spinning NMR of Half-Integer Quadrupolar Spins. *J. Magn. Reson.* **2017**, *277*, 131−142.
(53) Wi, S.; Schurko, R.; Frydman, L. Broadband Adiabatic Inversion Cross-Polarization Phenomena in the NMR of Rotating Solids. *Solid State Nucl. Magn. Reson.* **2018**, *94*, 31−53.
(54) Harris, R. K.; Becker, E. D.; Cabral de Menezes, M.; Goodfellow, R.; Granger, P. NMR Nomenclature : Nuclear Spin Properties and Conventions for Chemical Shifts. *Solid State Nucl. Magn. Reson.* **2002**, *22*, 458−483.
(55) Fayon, F.; Farnan, I.; Bessada, C.; Coutures, J.; Massiot, D.; Coutures, J. P. Empirical Correlations between 207Pb NMR Chemical Shifts and Structure in Solids. *J. Am. Chem. Soc.* **1997**, *119*, 6837−6843.
(56) Kidd, R. G. Nuclear Shielding of the Transition Metals. *Annu. Rep. NMR Spectrosc.* **1980**, *10*, 1−79.
(57) Mantsch, H. H.; Saitô, H.; Smith, I. C. P. Deuterium Magnetic Resonance, Applications in Chemistry, Physics and Biology. *Prog. Nucl. Magn. Reson. Spectrosc.* **1977**, *11*, 211−272.
(58) Bhattacharyya, R.; Frydman, L. Quadrupolar Nuclear Magnetic Resonance Spectroscopy in Solids Using Frequency-Swept Echoing Pulses. *J. Chem. Phys.* **2007**, *127*, 194503.
(59) Larsen, F. H.; Jakobsen, H. J.; Ellis, P. D.; Nielsen, N. C. Sensitivity-Enhanced Quadrupolar-Echo NMR of Half-Integer Quadrupolar Nuclei. Magnitudes and Relative Orientation of Chemical Shielding and Quadrupolar Coupling Tensors. *J. Phys. Chem. A* **1997**, *101*, 8597−8606.
(60) Bak, M.; Rasmussen, J. T.; Nielsen, N. C. SIMPSON: A General Simulation Program for Solid-State NMR Spectroscopy. *J. Magn. Reson.* **2011**, *213*, 366−400.
(61) Zaremba, S. Good Lattice Points, Discrepnacy, and Numerical Integration. *Ann. di Mater. Pura ed Appl.* **1966**, *73*, 293.
(62) Conroy, H. Molecular Schrödinger Equation. VIII. A New Method for the Evaluation of Multidimensional Integrals. *J. Chem. Phys.* **1967**, *47*, 5307−5318.

https://dx.doi.org/10.1021/acs.jpcc.0c04510
J. Phys. Chem. C 2020, 124, 14730−14744

(63) Harris, K. J.; Veinberg, S. L.; Mireault, C. R.; Lupulescu, A.; Frydman, L.; Schurko, R. W. Rapid Acquisition Of14N Solid-State NMR Spectra with Broadband Cross Polarization. *Chem. - Eur. J.* **2013**, *19*, 16469−16475.
(64) Veinberg, S. L.; Friedl, Z. W.; Harris, K. J.; O'Dell, L. A.; Schurko, R. W. Ultra-Wideline 14 N Solid-State NMR as a Method for Differentiating Polymorphs: Glycine as a Case Study. *CrystEngComm* **2015**, *17*, 5225−5236.
(65) Johnston, K. E.; O'Keefe, C. A.; Gauvin, R. M.; Trébosc, J.; Delevoye, L.; Amoureux, J.; Popoff, N.; Taoufik, M.; Oudatchin, K.; Schurko, R. W. A Study of Transition-Metal Organometallic Complexes Combining 35Cl Solid-State NMR Spectroscopy and 35Cl NQR Spectroscopy and First-Principles DFT Calculations. *Chem. - Eur. J.* **2013**, *19*, 12396−12414.
(66) O'Keefe, C. A.; Johnston, K. E.; Sutter, K.; Autschbach, J.; Delevoye, L.; Popoff, N.; Taoufik, M.; Oudatchin, K.; Schurko, R. W.; et al. An Investigation of Chlorine Ligands in Transition-Metal Complexes via 35 Cl Solid-State NMR and Density Functional Theory Calculations. *Inorg. Chem.* **2014**, *53*, 9581−9597.
(67) Hung, I.; Rossini, A. J.; Schurko, R. W. Application of the Carr−Purcell Meiboom−Gill Pulse Sequence for the Acquisition of Solid-State NMR Spectra of Spin- 1/2 Nuclei. *J. Phys. Chem. A* **2004**, *108*, 7112−7120.
(68) Schurko, R. W.; Hung, I.; Widdifield, C. M. Signal Enhancement in NMR Spectra of Half-Integer Quadrupolar Nuclei via DFS-QCPMG and RAPT-QCPMG Pulse Sequences. *Chem. Phys. Lett.* **2003**, *379*, 1−10.
(69) Hung, I.; Gan, Z. On the Practical Aspects of Recording Wideline QCPMG NMR Spectra. *J. Magn. Reson.* **2010**, *204*, 256−265.
(70) O'Dell, L. A. The WURST Kind of Pulses in Solid-State NMR. *Solid State Nucl. Magn. Reson.* **2013**, *55*−*56*, 28−41.
(71) Ashbrook, S. E.; Sneddon, S. New Methods and Applications in Solid-State NMR Spectroscopy of Quadrupolar Nuclei. *J. Am. Chem. Soc.* **2014**, *136*, 15440−15456.
(72) Ermakov, V. L.; Bohlen, J.-M.; Bodenhausen, G. Improved Schemes for Refocusing with Frequency-Modulated Chirp Pulses. *J. Magn. Reson., Ser. A* **1993**, *103*, 226−229.
(73) Pöppler, A. C.; Demers, J. P.; Malon, M.; Singh, A. P.; Roesky, H. W.; Nishiyama, Y.; Lange, A. Ultrafast Magic-Angle Spinning: Benefits for the Acquisition of Ultrawide-Line NMR Spectra of Heavy Spin- 1/2 Nuclei. *ChemPhysChem* **2016**, *17*, 812−816.
(74) Bak, M.; Rasmussen, J. T.; Nielsen, N. C. SIMPSON: A General Simulation Program for Solid-State NMR Spectroscopy. *J. Magn. Reson.* **2011**, *213*, 366−400.
(75) Cossement, C.; Darville, J.; Gilles, J.; Nagy, J. B.; Fernandez, C.; Amoureux, J. P. Chemical Shift Anisotropy and Indirect Coupling in SnO2 and SnO. *Magn. Reson. Chem.* **1992**, *30*, 263−270.
(76) Dybowski, C.; Neue, G. Solid State 207Pb NMR Spectroscopy. *Prog. Nucl. Magn. Reson. Spectrosc.* **2002**, *41*, 153−170.
(77) Janiak, C.; Schumann, H.; Stader, C.; Wrackmeyer, B.; Zuckerman, J. J. Decaphenylgermanocen, -Stannocen Und -Plumbocen Sowie Pentaphenylstannocen: Synthese, Eigenschaften Und CPMAS-Metall-NMR-Messungen. *Chem. Ber.* **1988**, *121*, 1745−1751.
(78) Kye, Y.-S.; Connolly, S.; Herreros, B.; Harbison, G. S. 207 Pb Solid State NMR Studies of Lead Compounds. *Main Group Met. Chem.* **1999**, *22*, 373−384.
(79) Vogt, F. G.; Gibson, J. M.; Aurentz, D. J.; Mueller, K. T.; Benesi, A. J. Multiple-Rotor-Cycle 2D PASS Experiments with Applications to 207 Pb NMR Spectroscopy. *J. Magn. Reson.* **2000**, *143*, 153−160.
(80) Schmidt-Rohr, K.; Spiess, H. W. *Multidimensional Solid-state NMR and Polymers*; Academic Press, Ltd.: London, U.K., 1994.
(81) Gath, J.; Hoaston, G. L.; Vold, R. L.; Berthoud, R.; Coperet, C.; Grellier, M.; Sabo-Etienne, S.; Lesage, A.; Emsley, L. Motional Heterogeneity in Single-Site Silica-Supported Species Revealed by Deuteron NMR. *Phys. Chem. Chem. Phys.* **2009**, *11*, 6962−6971.
(82) Vold, R. L.; Hoatson, G. L. Effects of Jump Dynamics on Solid State Nuclear Magnetic Resonance Line Shapes and Spin Relaxation Times. *J. Magn. Reson.* **2009**, *198*, 57−72.
(83) Iijima, T.; Nishimura, K. 2H Quadrupolar Carr-Purcell-Meiboom-Gill NMR for Paramagnetic Solids. *Chem. Phys. Lett.* **2011**, *514*, 181−186.
(84) Larsen, F. H.; Jakobsen, H. J.; Ellis, P. D.; Nielsen, N. C. Molecular Dynamics from 2 H Quadrupolar Carr−Purcell−Meiboom−Gill solid-state NMR spectroscopy. *Chem. Phys. Lett.* **1998**, *292*, 467−473.
(85) Groszewicz, P. B.; Breitzke, H.; Buntkowsky, G. Compensating the Asymmetric Probe Response in Broad MAS NMR Spectra of Quadrupolar Nuclei. *Solid State Nucl. Magn. Reson.* **2017**, *84*, 227−233.
(86) Jeener, J.; Broekaert, P. Nuclear Magnetic Resonance in Solids: Thermodynamic Effects of a Pair of Rf Pulses. *Phys. Rev.* **1967**, *157*, 232−240.
(87) Barbara, T. M.; Vold, R. L.; Vold, R. R. A Modified Jeener-Broekaert Sequence for Relaxation Measurements in Liquid Crystals. *J. Magn. Reson.* **1984**, *59*, 478−484.
(88) Wimperis, S.; Bodenhausen, G. Broadband Excitation of Quadrupolar Order by Modified Jeener-Broekaert Sequences. *Chem. Phys. Lett.* **1986**, *132*, 194−199.
(89) Charpentier, T.; Sakellariou, D.; Virlet, J.; Dzheparov, F. S.; Jacquinot, J. F. Nuclear Spin Dynamics Using Time-Dependent Projection Operators: Application to the Saturation of Dipolar Order in Slowly Rotating Samples. *J. Chem. Phys.* **2007**, *127*, 224506.
(90) Müller, C.; Schajor, W.; Zimmermann, H.; Haeberlen, U. Deuteron Chemical Shift and EFG Tensors in α-Glycine. *J. Magn. Reson.* **1984**, *56*, 235−246.
(91) Gan, Z.; Robyr, P. Deuterium Polarization Transfer in Rotating Solids and Its Application in Structural Investigation. *Mol. Phys.* **1998**, *95*, 1143−1152.
(92) Aliev, A. E.; Mann, S. E.; Rahman, A. S.; McMillan, P. F.; Corà, F.; Iuga, D.; Hughes, C. E.; Harris, K. D. M. High-Resolution Solid-State 2H NMR Spectroscopy of Polymorphs of Glycine. *J. Phys. Chem. A* **2011**, *115*, 12201−12211.

https://dx.doi.org/10.1021/acs.jpcc.0c04510
J. Phys. Chem. C 2020, 124, 14730−14744